A NUMERICAL STUDY OF INCOMPRESSIBLE FLUID FLOW OVER A FORWARD FACING STEP AT VARIOUS GRADES

by

PETER ANDREW MARTINEZ

Presented to the Faculty of the Graduate School of

The University of Texas at Arlington in Partial Fulfillment

of the Requirements

for the Degree of

MASTER OF SCIENCE IN MECHANCIAL ENGINEERING

THE UNIVERSITY OF TEXAS AT ARLINGTON

May 2013

Acknowledgements

I would like to thank my supervising professor Dr. Albert Y. Tong for his continuing support throughout my academic career and for continually motivating me to reach for my absolute highest potential. I would also like to give a special thanks to my committee members, Dr. Abdolhossein Haji-Sheikh and Dr. Seiichi Nomura, for their time and support in my research. I would also like to mention Debi Barton, Yin Guan, Daipayan Sarkar, and Vimal Ramanuj, who were all very helpful in guiding me during my research. Finally, I would like to express my gratitude to my family, for their constant support, encouragement, and patience.

April 19, 2013

Abstract

A NUMERICAL STUDY OF INCOMPRESSIBLE

FLUID FLOW OVER A FORWARD

FACING STEP AT VARIOUS

GRADES

Peter Andrew Martinez, M.S.

The University of Texas at Arlington, 2013

Supervising Professor: Albert Y. Tong

The study of the effect of natural forces on hydraulic structures is of great concern for the accurate prediction when a design could be at risk of failure. In recent times the use of the shallow water equations to predict the behavior of the free surface for flow over a step has proven inaccurate because only a hydrostatic pressure distribution is considered. One of the phenomena that will not be accounted for with the shallow water equations in such a setup is the formulation of undular bore type waves on the surface. For a more accurate representation of the behavior of the free surface a computational flow solver must be used with a more accurate method. A numerical study has been performed in this research to investigate the behavior of the free surface in open channel flow over a forward facing step at multiple stream gradients.

Table of Contents

List of Illustrations

List of Tables

Chapter 1

Introduction

1.1 Objective

The study of the effect of natural forces on hydraulic structures is of great concern for the accurate prediction when a design could be at risk of failure. It has been shown by Bukreev and Gusev [1] that in considering the problem of a dam break the use of the shallow water equations for the calculation model will not always be accurate. This is because the shallow water equations will not account for the formulation of undular bore type waves on the surface. The reason that Bukreev and Gusev found the shallow water equations to be incomplete is because these equations only consider a hydrostatic pressure distribution, and so the experiments in [1] focused on the flow over an obstacle such as a step where a non-hydrostatic condition could occur even during a steady state. A numerical study that simulated similar experimental conditions was conducted by Khazhoyan and Khakimzyanov [2] which used a finite-difference algorithm based on the ideal potential flow model to approximately predict the behavior of the free surface over a step.

There are many practical applications that can benefit from the study of a flow over an obstacle such as a step. Besides hydraulics and dam analysis, these studies have been found to be useful for the analysis of medical devices like an oxygenator [3] where a similar physical setup like this can occur. The obstacle is very useful for increasing the heat transfer coefficient in the area of the step by causing a swirl of fluid to occur as it flows past the step. There are numerous other studies which analyze the flow over a step but there are very few that take into account the effect of stream gradient for a more realistic flow situation. The objective of the present study is to determine the effect of stream gradient on the free surface for an incompressible fluid flow over a step.

In order to study the free surface the channel flow will be numerically simulated using an algorithm that combines the advantages of the level set and volume of fluid methods. This combined method is called a coupled level set and volume-of-fluid (CLSVOF) method. Using this method to obtain the free surface at steady state, we can observe the correlation between the change in stream gradient and other parameters like the Froude number or step height.

1.2 Background Literature Review

1.2.1 Experimental Studies

There have been many studies which have been done to determine the behavior of a flow encountering an obstacle. In [4], Sutherland and Aguilar performed experiments with stratified flow over 2D obstacles shaped like a sine wave, rectangle, and triangle. These types of topography are encountered in air flow over mountainous terrain or on the ocean floor and thus are of interest for scientific studies. Martinuzzi and Tropea [5] experimented with channel flow around prismatic obstacles and their results give a good understanding of what sort of behavior can occur with three-dimensional geometry in fully developed flow. These experimental works are important because they give better insight on the separation zone that tends to occur near an obstacle such as a step. This separation zone is a key phenomenon that causes some differences in the numerical and experimental studies and will be discussed later. By viewing the flow in a 3D geometry the behavior of this separation zone can be fully seen and clearly understood. Heinrich Stüer [6] has examined in his research the differences between closed and open separation zones that occur during 2D and 3D flows over a forward facing step. The flow that will be simulated in the experiments of this particular study is a 2D flow.

In the experiments of [1], Bukreev and Gusev use a measuring needle to measure different data points to track the free surface of a flow across a step in a

rectangular channel. The flow rate was measured by either a volumetric method or a Venturi tube depending on the flow rate. Another key difference between the experiments and the numerical simulations that were performed is that the flow in the experiments was allowed to spill over into the atmosphere at the exit. A separation zone is also observed with several vortices at the bottom of the front face of the step in the experiments. It is this flow separation that the authors of [1] believe to be one of the causes of the undular bore type behavior that develops over the step at the free surface.

1.2.2 Numerical Studies

There are several numerical studies that exist that examine open channel flow across a step. In one such study [7], a flow over a sill is simulated using the immersed boundary method (IBM) which was initially developed to create a numerical simulation to study the flow of blood in the human heart. The immersed boundary method is especially useful for flows that pass over an obstacle that will deform due to the flow. The value of the IBM is that it is able to handle the task of calculating the change in the boundary as a result of the flow and simultaneously the change in flow as a result of the moving boundary condition that makes up the free surface. This is a coupled solution that the IBM is able to handle much easier than other methods.

When analyzing the response of an incompressible fluid to gravitational and rotational forces the shallow water solutions are commonly employed because they work well in situations where the horizontal length scale is significantly greater than the vertical scale. These equations were first developed by a French mathematician by the name of Jean Claude Saint-Venant during the 19^{th} century. These equations were further refined to take into account non-hydrostatic pressure contributions by the addition of a dispersive term. The Green–Naghdi equations are a particular set of shallow water equations using this dispersive form and were first derived by Sulu and Gardner [8] but were later refined

and derived subsequently by many others. A study by Nadiga, Margolin, and Smolarkiewicz [9] compares the differences in the different approximations for flow over an obstacle using the shallow water solutions, the dispersive shallow water solutions, and the Green–Naghdi equations.

1.3 Interface Tracking Techniques Background

The main difficulty of numerically simulating a flow with a free surface is that a rapidly moving irregular interface is undergoing complex topological changes, and must be located and tracked. In order to accomplish this task there are several methods available that may be implemented. Two of these methods will be discussed and examined to see their strengths and weaknesses. The first of these methods is the volume-of-fluid (VOF) method, and the second is the level set (LS) method.

1.3.1 The Volume of Fluid (VOF) Method

The marker and cell (MAC) technique was developed by Francis Harlow and Los Alamos National Laboratory [10], and was used in computational fluid dynamics as a way to simulate fluid flow by using particles called markers to track the fluid flow. The basic concept of the MAC technique is that space is broken up into tiny grid cells which are used to determine the velocity and pressure while the marker particles instruct the computer which cells contain fluid. This concept was taken further by the development of the Volume of Fluid (VOF) method which first appeared in 1976 [11], and was later published in [12]. In this method the interface of the fluid is tracked by a scalar fractional function C ($\vec{x}$,t) which is defined as:

$$C(\vec{x},t)=\begin{cases}1, & \text{in the fluid}\\ 0<C<1, & \text{at the interface}\\ 0, & \text{in the void}\end{cases} \tag{1.1}$$

Now the data each cell contains is a fractional representation of the amount of fluid in the cell. A sample set of data that is commonly found in a VOF array is shown in Figure 1.1. This data alone does not tell us exactly where the free surface is located so as an example of how this data would be used to reconstruct the interface a square drop has been reconstructed using the Nichol-Hirt (NH) algorithm from [12], and is shown in Figure 1.2. The NH scheme is the most basic version of VOF, and uses only vertical and horizontal lines to track the interface. The interface for the square drop that was produced is not a unique solution because it was based on the scheme that was chosen to reconstruct the interface. This interface only really needs to meet the condition that each cell contains the fraction of fluid volume indicated by its C ($\vec{x}$,t) value and thus different interface tracking schemes could each result in a different interface that is also equally valid.

The example of the square drop is only for the purpose of demonstrating the method used in reconstructing the interface. In actual testing the geometry of a numerical simulation is usually far more complicated than this. As the free surface moves it is

0.0	0.0	0.0	0.0	0.0
0.0	0.25	0.50	0.25	0.0
0.0	0.50	1.00	0.50	0.0
0.0	0.25	0.50	0.25	0.0
0.0	0.0	0.0	0.0	0.0

Figure 1.1 A sample of data contained in an array using the VOF method.

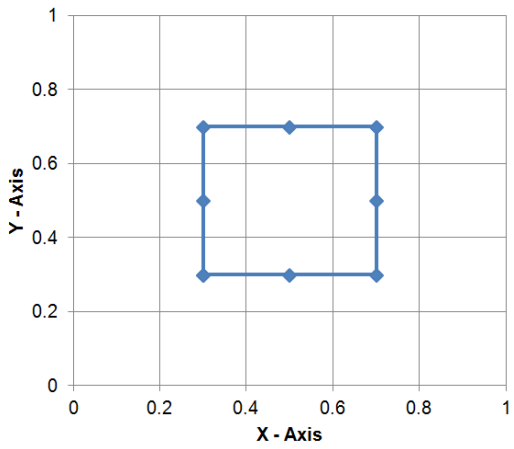

Figure 1.2 A square drop interface reconstructed using the most basic version of VOF the Nichol-Hirt scheme.

necessary to recalculate the interface location at each time step in the calculation cycle which is what the NH algorithm would do. The Piecewise Linear Interface Calculation (PLIC) scheme [13] would later replace the NH Algorithm and was able to produce an interface that was free of the imperfections the NH algorithm would generate. The PLIC scheme works by taking all cells that contain the interface and uses the gradient of C ($\vec{x}$,t) to compute a normal vector $\vec{n}$ in each cell. Then using this directional vector an interface is constructed in each cell by a straight line that divides the cell according to its fractional C ($\vec{x}$,t) value. The VOF version using the PLIC scheme is a far more accurate tool to track the free surface.

1.3.2 The Level Set (LS) Method

Another method that has been used in interface tracking is the level set method which was created by a pair of American mathematicians named James Sethian and Stanley Osher [14, 15] during the late 1980's. The LS method works well with tracking interfaces or complex shapes that change topology. The LS function also is very useful because it contains the property that the magnitude of the gradient of the LS function is

equal to one. This property can be used to simplify other equations. The LS method uses a signed distance function φ which represents the interface when the function takes a value of zero and then for other values the magnitude of the function also represents the shortest distance to the interface. It is defined as follows:

$$\varphi(\vec{x},t) = \begin{cases} > 0, & \text{outside the interface} \\ = 0, & \text{at the interface} \\ < 0, & \text{inside the interface} \end{cases} \tag{1.2}$$

As per the function's definition, the inside of the fluid is represented by negative φ values and the outside is located where the values are positive. To illustrate this a sample set of data is shown in Figure 1.3 for another square drop but this time more cells are added to help to make clear the function of the LS method. The cells which are inside of the free surface of the fluid are shaded blue in the sample data and as can be seen contain only negative values. The free surface that is produced from this data is shown in Figure 1.4. The LS function will fail to be a distance function after the interface has been advected, and as a result the magnitude will no longer be equal to one. To correct this

0.354	0.292	0.255	0.250	0.250	0.250	0.250	0.255	0.292	0.354
0.292	0.212	0.158	0.150	0.150	0.150	0.150	0.158	0.212	0.292
0.255	0.158	0.071	0.050	0.050	0.050	0.050	0.071	0.158	0.255
0.250	0.150	0.050	-0.050	-0.050	-0.050	-0.050	0.050	0.150	0.250
0.250	0.150	0.050	-0.050	-0.150	-0.150	-0.050	0.050	0.150	0.250
0.250	0.150	0.050	-0.050	-0.150	-0.150	-0.050	0.050	0.150	0.250
0.250	0.150	0.050	-0.050	-0.050	-0.050	-0.050	0.050	0.150	0.250
0.255	0.158	0.071	0.050	0.050	0.050	0.050	0.071	0.158	0.255
0.292	0.212	0.158	0.150	0.150	0.150	0.150	0.158	0.212	0.292
0.354	0.292	0.255	0.250	0.250	0.250	0.250	0.255	0.292	0.354

Figure 1.3 A sample of data that is used to create a square drop using the LS method.

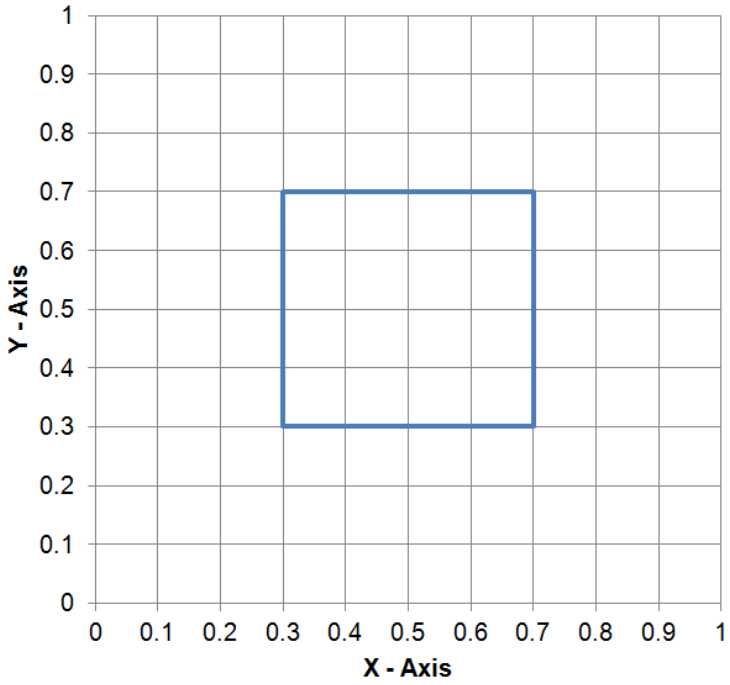

Figure 1.4 A graph of the interface for the square drop that is produced from the sample data in Figure 1.3

error the LS function must then be reinitialized in order to reestablish it as a distance function again; however, this will not guarantee that mass will be conserved.

1.4 The Continuum Surface Force (CSF) Method

The modeling of surface tension is another problem that usually requires some attention for most numerical simulations [16]. In this particular study it is assumed the effect of surface tension forces is of minor concern. It is only for the purpose of disclosure that the Continuum Surface Force (CSF) method is mentioned here to explain the treatment of surface tension in the model. In summary, the CSF method treats surface tension as a body force that is distributed through a transition region of a finite thickness.

1.5 Scope of the Research

This study was focused on investigating the effect of the stream gradient on the free surface in the region above a step. The coupled level set and volume of fluid (CLSVOF) method is employed to track the free surface in the numerical simulations of this study. The CLSVOF method will be covered in detail to explain its significance and the way in which calculations are performed to create the simulation. In this study the flow is viscous with a mix of slip and no-slip boundary conditions. In the future, further studies could be done to examine if further refinement to the boundary conditions would make a difference in improving the results. A realistic range of downhill slopes was tested and compared to a no slope profile. The results were then analyzed to determine the effect caused to the free surface in response to changes in stream gradient as well as the correlation to changes in the velocity and step height. As has been mentioned before, when the shallow water equations are used to model a flow it is only an approximation that simplifies the flow to a one dimensional problem. The cost of simplifying the equations is that the model is not able to handle an obstacle in the flow such as a step where the flow velocity in the vertical direction cannot be ignored. The methods used in this study improved upon the shallow water model, and allowed the behavior of the free surface over a forward facing step to be determined with reasonable accuracy.

1.6 Organization of the Thesis

In Chapter 2 the CLSVOF is explored in more detail to understand its significance to the research to be conducted in this study. In Chapter 3 the numerical setup is explained for the simulations that will be run. Some introductory terminology is introduced also in Chapter 3 as well as an explanation of some of the boundary conditions. In Chapter 4 the results of the studies on stream gradient for flow over a step

are presented and discussed further. In the final Chapter, the conclusions of this research are stated and suggestions for future work and studies are explored.

Chapter 2

Numerical Formulation

2.1 Introduction

Numerical methods can be used to simulate a realistic physical process like a river flow or hydraulic waves near a dam associated with a hydroelectric water power facility. In the case of open channel flow the free surface presents a problem because it is classified as a moving boundary problem. The numerical techniques used to simulate a particular case for study must be carefully picked to make sure they will accurately reflect a real experiment. Once an appropriate method has been chosen and tested to make sure it reflects experimental data accurately then that numerical model becomes a powerful tool to test other conditions. In this study it has already been mentioned that a CLSVOF method will be used, but the method of implementation of the code is not unique. There are other algorithms for the PLIC scheme and re-distance implementation schemes that have been formulated besides the specific code used in this study. Now that some of the earlier numerical methods have been briefly covered the CLSVOF method can be covered in detail to illustrate the significance of its selection for this study as well as to understand its strengths and limitations.

2.2 Governing Equations

It has already been stated before that the calculation of the flow with a free surface presents in itself a difficult class of moving boundary problem. The interface that is to be tracked has a mathematical discontinuity, and determining the velocity and pressure is very challenging. It is thus necessary to use special methods as well as a flow solver to track the movement of the free surface and determine its location. The computer code that will be used in this study will be adopting a finite difference method (FDM) for solving the incompressible Navier-Stokes equation. The free surface will be tracked with

VOF data on the cell and is reconstructed with a piecewise linear interface calculation scheme. The curvature and normal will be estimated with the level set method, and both methods will be combined in CLSVOF scheme to reconstruct the free surface in the channel flow. The computer code that is used models a 2D flow in an Eulerian frame. The governing equation is the continuity equation for incompressible flow, (2.1)

$$\nabla \cdot \vec{V} = 0$$

and the momentum equation:

$$\frac{\partial \vec{V}}{\partial t} + \nabla \cdot (\vec{V}\vec{V}) = -\frac{1}{\rho}\nabla p + \frac{1}{\rho}\nabla \cdot \tau + \vec{g} + \frac{1}{\rho}\vec{F}_b \tag{2.2}$$

where the velocity is $\vec{V}$, density is ρ, pressure is p, the viscous stress tensor is τ, the gravitational acceleration is $\vec{g}$, and the body force is $\vec{F}_b$. If the fluid is a Newtonian fluid the viscous stress tensor, τ, can be written as:

$$\tau = 2\mu S \tag{2.3}$$

where the dynamic viscosity is written as μ and the strain tensor S is equivalent to:

$$S = \frac{1}{2}\left[(\nabla \vec{V}) + (\nabla \vec{V})^T\right] \tag{2.4}$$

The first step that is needed for the flow solving algorithm is to discretize the momentum equation which results in:

$$\frac{\vec{V}^{n+1} - \vec{V}^n}{\delta t} = -\nabla \cdot (\vec{V}\vec{V})^n - \frac{1}{\rho^n}\nabla p^{n+1} + \frac{1}{\rho^n}\nabla \cdot \tau^n + \vec{g}^n + \frac{1}{\rho^n}\vec{F}_b^n \tag{2.5}$$

The superscripts n and n+1 are used to represent the value of the associated variable at consecutive time steps. The pressure is the only implicit term that is used in Equation 2.5. Besides the velocity $\vec{V}$, the other remaining terms will need to be approximated with the old time t^n values. The next step involves separating Equation 2.5 into two separate equations by the use of a two-step projection method [17]:

$$\frac{\vec{\tilde{V}}-\vec{V}^n}{\delta t} = -\nabla\cdot(\vec{V}\vec{V})^n + \frac{1}{\rho^n}\nabla\cdot\tau^n + \vec{g}^n + \frac{1}{\rho^n}\vec{F}_b^n \quad (2.6)$$

$$\frac{\vec{V}^{n+1}-\vec{\tilde{V}}}{\delta t} = -\frac{1}{\rho^n}\nabla p^{n+1} \quad (2.7)$$

A new term is introduced by the separation process that is called the intermediate value of velocity and is denoted by the symbol $\vec{\tilde{V}}$. In the first stage of the projection method, the intermediate velocity field, $\vec{\tilde{V}}$, is solved from the previous time step after the effects of advection, viscosity, gravity, and body forces have been accounted for. In the second stage, the velocity field, $\vec{V}^{n+1}$, is projected onto a divergence free vector field by combining Equation 2.7 and the discretized continuity equation:

$$\nabla\cdot\vec{V}^{n+1} = 0 \quad (2.8)$$

which results in a pressure Poisson equation (PPE):

$$\nabla\cdot\left[\frac{1}{\rho^n}\nabla p^{n+1}\right] = \frac{\nabla\cdot\vec{\tilde{V}}}{\delta t} \quad (2.9)$$

This equation can be solved by using an incomplete Cholesky conjugate gradient (ICCG) method [18] and will produce the vector field for the next time step, t = n+1.

2.3 The Coupled Level Set and Volume of Fluid Method

It has already been discussed in the previous chapter the strengths and weaknesses of the VOF and level set methods. It is by combining these two methods into one that it is possible to create the improved CLSVOF method which is able to track the free surface far more accurately. This method will use the VOF function in Equation 1.1 to reconstruct the interface with a PLIC scheme, and calculate the normal of the interface from the LS function shown in Equation 1.2. As already mentioned, the level set function may require some re-distancing to return the function to a distance function after advection. The result of these combined methods is that the curvature and normal of the interface is computed with more accuracy and that it is still possible to maintain accurate

mass conservation. The CLSVOF can be thus examined in two parts. In the first part the VOF function is used for volume tracking, and in the second part the LS function is used for calculating the local curvature and the normal vector.

2.3.1 The VOF Part - Volume Tracking

The VOF function of Equation 1.1 is advanced through the following propagating equation:

$$\frac{\partial C}{\partial t} + (\vec{V} \cdot \nabla) C = 0 \tag{2.12}$$

In order to ensure that that mass conservation is preserved, Equation 2.12 can be rewritten in the conservative form:

$$\frac{\partial C}{\partial t} + \nabla \cdot (\vec{V} C) = C(\nabla \cdot \vec{V}) \tag{2.13}$$

This equation is next decomposed into two fractional steps, and for the two-dimensional case the result is the following two equations:

$$\frac{\tilde{C} - C^n}{\delta x} + \frac{\partial}{\partial x}(uC^n) = \tilde{C}\frac{\partial u}{\partial x} \tag{2.14}$$

$$\frac{C^{n+1} - \tilde{C}}{\delta t} + \frac{\partial}{\partial x}(v\tilde{C}) = \tilde{C}^{n+1}\frac{\partial v}{\partial y} \tag{2.15}$$

The symbol $\tilde{C}$ is used indicate an intermediate VOF function value. In Figure 2.1 the grid setup for a cell is shown which depicts a staggered grid that is used to calculate the velocity components at the cell faces and the pressure, VOF, and LS functions at the cell centers. The next step is to discretize according to Figure 2.1 the two decomposed equations which results in:

$$\tilde{C}_{i,j} = \frac{C_{i,j}^n \delta x_i \delta y_j - \delta t \delta y_j \{(uC^n)_{i+1/2,j} - (uC^n)_{i-1/2,j}\}}{\delta x_i \delta y_j - \delta t \delta y_j \left(u_{i+\frac{1}{2},j} - u_{i-1/2,j}\right)} \tag{2.16}$$

$$C_{i,j}^{n+1} = \frac{\tilde{C}_{i,j}^{n}\delta x_i \delta y_j - \delta t \delta x_i \{(v\tilde{C})_{i,j+1/2} - (v\tilde{C})_{i,j-1/2}\}}{\delta x_i \delta y_j - \delta t \delta x_i \left(v_{i,j+\frac{1}{2}} - v_{i,j-1/2}\right)} \quad (2.17)$$

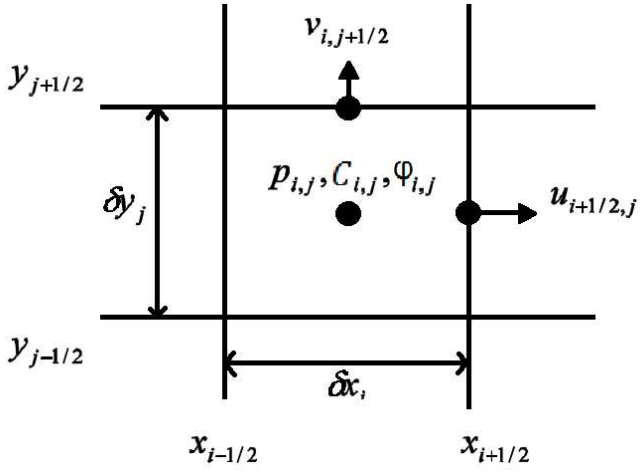

Figure 2.1 A grid cell setup showing the locations that the governing equations are applied to. This configuration is known as a staggered grid setup.

These equations will both be used during interface reconstruction by the PLIC algorithm to calculate the VOF fluxes across each grid cell that contains an interface.

2.3.2 The LS Part – Local Curvature and the Normal Vector

The second part of the CLSVOF method involves using the LS function to calculate the local curvature and normal vectors of each cell containing a portion of the interface. The governing equation that allows the LS method that was given in Equation 1.2 to be advected is:

$$\frac{D\varphi}{Dt} = \frac{\partial \varphi}{\partial t} + \left(\vec{V} \cdot \nabla\right)\varphi = 0 \quad (2.17)$$

In order to maintain that the LS function continues to be a distance function after advection the following re-initialization process [19] has been applied:

$$\frac{\partial \varphi}{\partial \tau} = \frac{\varphi_0}{\sqrt{\varphi_0^2 + h^2}}(1 - |\nabla \varphi|) \tag{2.18}$$

where φ_0 is the level set function of the previous time step, h is the grid width, and τ is the artificial time. The details of the specific algorithm that is used to re-distance the LS function can be found in [20]. In this study the normal vector to the interface is estimated by the following equation:

$$\vec{n} = \frac{\nabla \varphi}{|\nabla \varphi|} = \nabla \varphi \tag{2.19}$$

The local curvature at the interface is computed by the following equation:

$$\kappa = \nabla \cdot \nabla \varphi \tag{2.20}$$

Now that both parts of the CLSVOF have been discussed the entire process of the CLSVOF implementation can be readily seen in Figure 2.2. Testing conducted by Wang in [21] revealed that the CLSVOF is far superior to the LS method alone as demonstrated in a slotted disc and circular shearing advection test. It is also shown in that same study that the advantage of the CLSVOF over the VOF is that spurious currents are greatly reduced when the CSLVOF is used with the CSF method. This improvement in the accuracy of tracking the interface does come with a price which is that more computational time and memory is used because both the VOF and LS function each have to be calculated in this method.

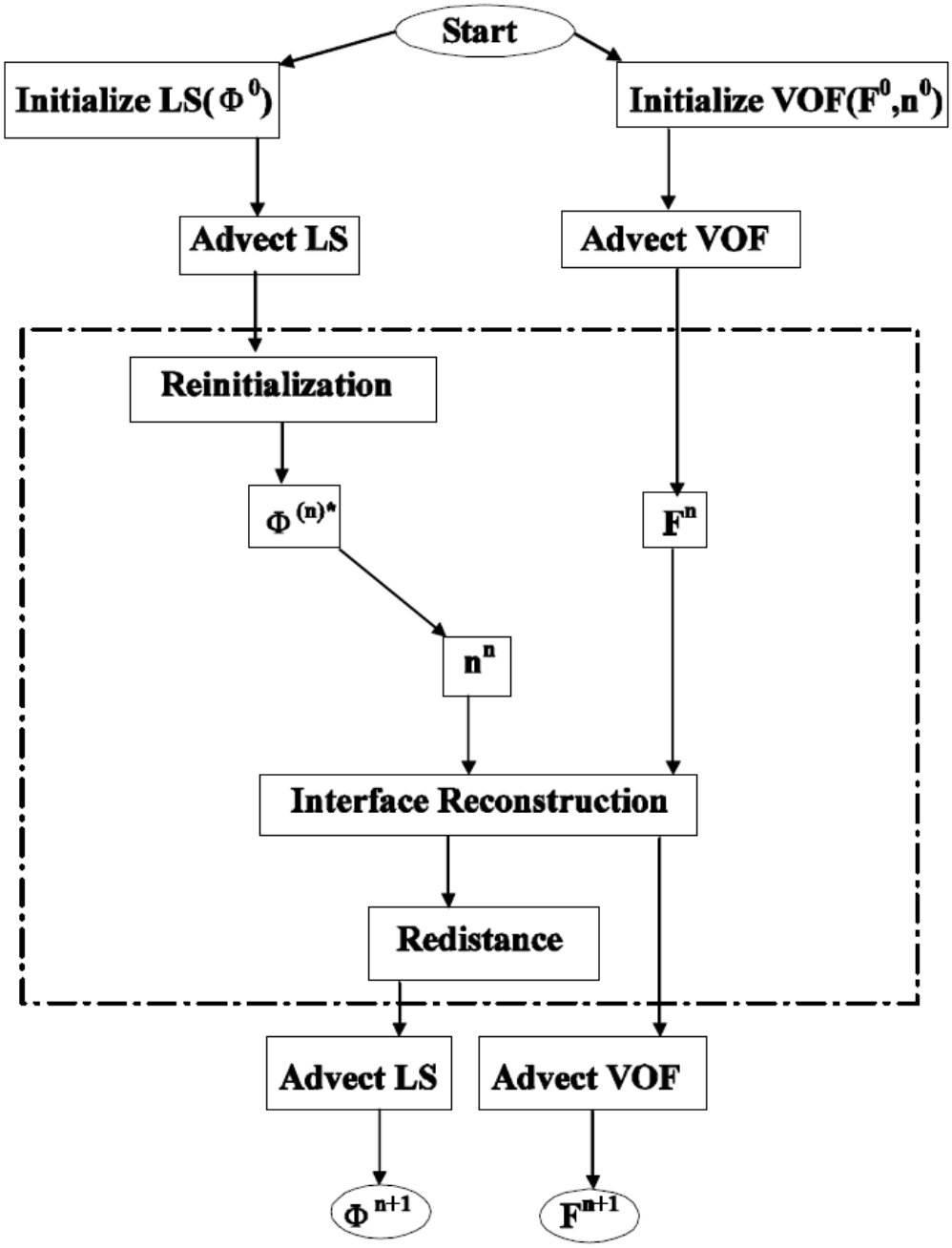

Figure 2.2 A detailed flow chart of the CLSVOF algorithm.

Chapter 3

Numerical Experiment Setup

3.1 Introduction

This study is concerned with free surface flow which is a type of flow that happens when part of the flow is not in contact with anything but a void of space. The interface exposed is called a free surface because that particular boundary is able to deform and change shape. When considering the boundary conditions for the interface for this particular type of flow it is assumed that both the shear stress and pressure are equal to zero at the free surface. Strictly speaking the flow that occurs in nature does not meet this condition and is actually considered a two phase flow. This is because the interface of the fluid is in contact with another fluid which is the air, but the large degree of difference between the densities of air and water allow us neglect the effects of the air in the atmosphere. A free surface flow of the type shown in Figure 3.1 is generally found to be flowing downhill and thus the stream gradient will be an important consideration in

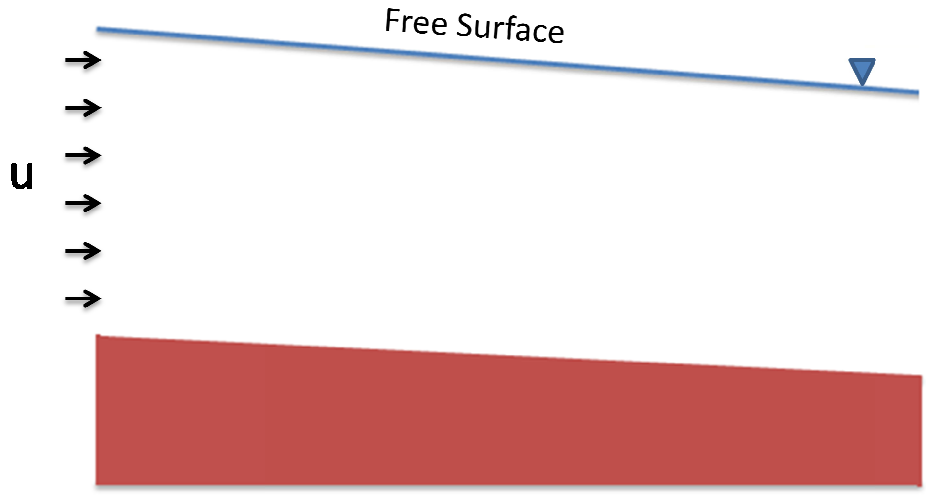

Figure 3.1 A free surface flow.

any serious free surface flow study.

3.2 Steam Gradient

The stream gradient is the measure of the rate of which the elevation in a stream is changing with respect to the horizontal length. The stream gradient is determined by first taking a measurement of the elevation of the bed of the flow at an upstream and downstream location. The stream gradient is then the result of the ratio of the effective height (H) to the horizontal distance (L) as shown in a sample calculation in Figure 3.2. In this particular study the focus is on the effect of stream gradient on the free surface in the vicinity of a step, but there are many other purposes to modeling stream gradient besides this. It can be used as a way to predict fluvial geomorphology [22], to estimate the local distribution of the populations of several aquatic organisms based on spawning habits, and it is also used to determine where debris will be deposited by the flow of the channel. Looking at several different types of channel classifications used in [23] for the streams found in Oregon it is possible to categorize the slopes into three categories in order that this study will be using a realistic range of stream gradients. Table 3.1 shows the range of slopes found for some channels in [23] and also gives a description of some of the

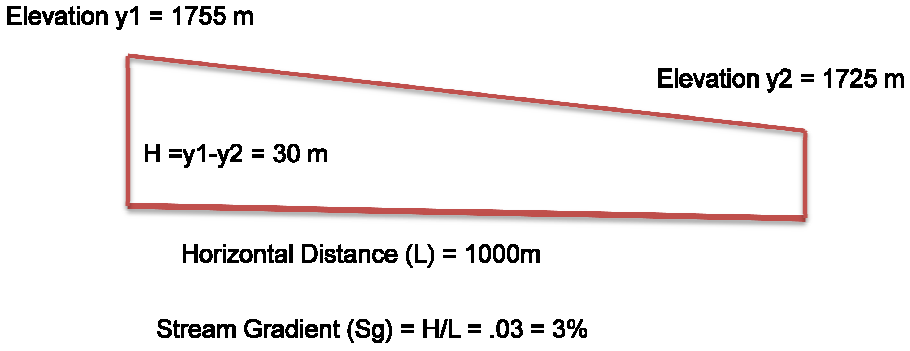

Figure 3.2 A sample calculation of a stream gradient.

Table 3.1 Data for Different Channel Types Found in [23].

Type	Stream Gradient	Channel Types	Types of Shapes of these Valleys	Substrates
Low	Sg < 1.5%	Small Estuarine, Low Gradient Large Floodplain	Broad, Floodplain	Sand, Cobble, Small Gravel
Moderate	1.5% < Sg < 4.0%	Low Gradient Medium Floodplain, Low Gradient Small Floodplain, Low Gradient Confined Channel, Moderately Gradient Moderately Confined	Broad, Flat, Narrow, Gentle Landforms, Limited Floodplain	Gravel, Boulders, Cobble, Bedrock, Sand
Steep	Sg > 4.0%	Moderately Steep Narrow Valley, Bedrock Canyon	Gentle to Narrow V-Shaped Valley, Canyons, Gorges, Steep Slopes	Bedrock, Boulders, Cobble

valley types and substrate that can be found there as well. The range of slopes for this study will be selected from the low to moderate stream gradients

3.3 Numerical Experiment Setup

Figure 3.3 shows the layout of the numerical experiment for each of the simulations that were performed. The characteristic length for this study is the height of free surface (h_0) at the initial time t = 0, and this value is set to be 145.5 mm as specified in the experiments of [1] and [2]. The computational domain is laid out over a region that is $X2$ by Y. The distance of $X2$ is normalized and set to be equal to x/h_0 = 30. The value of $X2$ was set to be the same distance in each of the simulations. The value of $Y2$ is adjusted as needed based on the expected growth of the pressure head after the simulation begins. The step height (B) of the obstacle is also normalized, and varies from B/h_0 = 0.2222 to B/h_0 = 0.5 depending on the simulation that was tested.

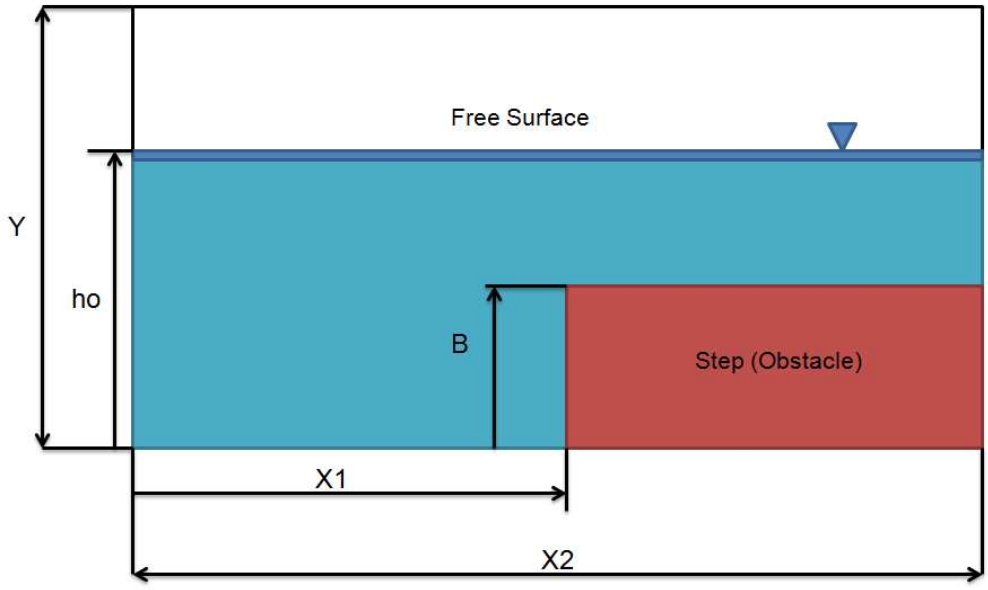

Figure 3.3 Numerical experiment setup at time t =0. (Not drawn to scale)

3.3.1 The Boundary Conditions of the Numerical Simulation

The boundary conditions of the computational domain are shown in Figure 3.4. At the inlet side there are two boundary conditions that are implemented. The first boundary condition BC1 is set to specified inflow with an inlet velocity (U_{-inf}) that is prescribed according to the desired flow velocity for each simulation that is to be tested. This boundary condition is applied for all the cells that are along the side of the domain up until the height of the initial free surface (h_0). The second boundary condition (BC2) begins where BC1 ends and includes the remaining cells on the left hand side of the domain. The velocity components of the cells found in the BC2 region are each set to be equal to zero. The boundary conditions of BC1 and BC2 are constant throughout the rest of the simulation. These boundary conditions along the inlet limited the range of testing, but as long as the parameters were specified within a proper range the accuracy of the simulation was not affected. The inlet condition of boundaries BC1 and BC2 will be further addressed in Chapter 5. At the top and bottom of the domain the boundary

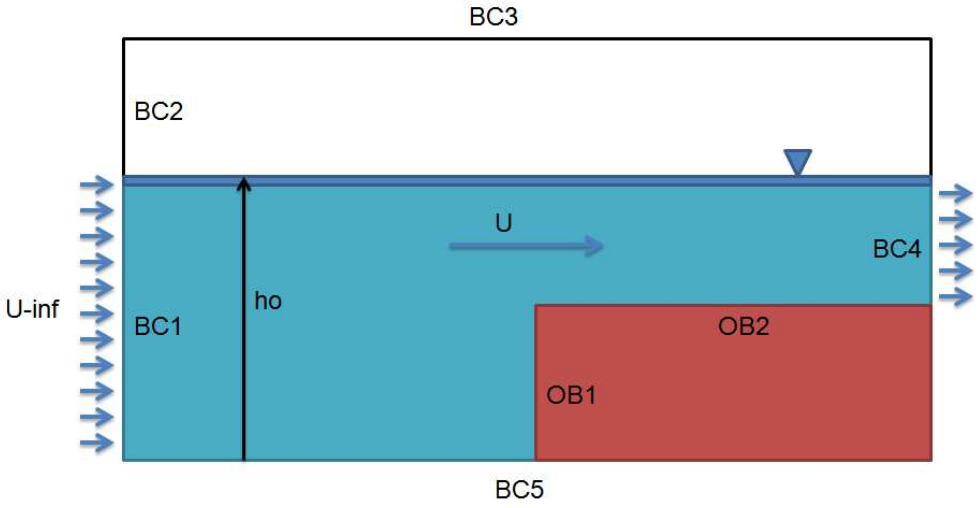

Figure 3.4 Boundary conditions of the computational domain in the experiments.

condition (BC3 & BC5) is the same which is a rigid no-slip condition across these cells. This does create a temporary ceiling for the simulation when it begins, but the height is carefully specified in order that the presence of this boundary is meaningless at steady state. The boundary condition at the outlet side is specified as continuative outflow which will enforce the condition that all normal derivatives at the boundary are zero. Within the domain another type of boundary condition exists at the surfaces of the obstacle located at OB1 and OB2. At these locations a rigid free-slip boundary is prescribed. Finally, the initial velocity (U) of the fluid contained in the domain is set to the same value as the inlet condition at BC1. It should also be noted that the frame of reference for each simulation is with the computational domain running parallel to the bottom of the channel. This allows each simulation to have an increasing stream gradient simply by redefining the direction of the gravitational vector.

Chapter 4

Results

4.1 Introduction

Three separate series of studies were performed in order to determine the effect of a change in stream gradient on the free surface for flow over a step. Flow classification and the critical depth will need to be discussed first in order to appreciate the significance of these studies. A grid refinement study was first completed in order to validate the numerical results and determine the appropriate grid size. A preliminary set of simulations were also performed and compared to previous results to check to see if the selected testing range would be able to produce accurate results given the boundary conditions. The results of the three studies will be presented and discussed separately to examine their significance.

4.2 Classification of Flow

It is important to discuss flow classification because it will help to provide one method of defining the initial inlet conditions as well provide an important parameter that will be used in testing which is the Froude Number. In dealing with open-channel flow there are two ways of classifying the flow. The first is by classifying the flow according to the slope of the free surface. If the free surface of the flow is running a long path that is at constant velocity and depth then the flow is said to be in uniform flow. If the depth of the flow or velocity changes slowly over time the flow is said to be gradually varied, and can be approximated in analysis by a first order differential equation. However, if there is an obstacle or change in the cross section of the flow that causes the depth to change greatly over a short distance then the flow will be said to be a rapidly varied flow and will

have to be analyzed through numerical analysis or experimentation. A description of the different classifications of flows by depth variation is shown in Figure 4.1.

The second method of flow classification is the Froude number, Fr, which is a dimensionless parameter that is the ratio of the velocity of the flow to the propagation speed of waves in the flow. The Froude number is defined by the following equation

$$Fr = \frac{U}{\sqrt{gy}} \tag{4.1}$$

where the velocity of the flow is U, acceleration due to gravity is g, and the depth of the flow in the channel is y. The denominator term $\sqrt{gy}$ is the speed of an infinitesimal shallow water surface wave, and this ratio will allow us to predict which direction waves would propagate if a disturbance like a rock was thrown into the flow. The Froude number can thus predict the direction that ripples caused by the rock would be able to travel as shown in Table 2.

4.3 Critical Depth

No study on open channel flow would be complete without taking into

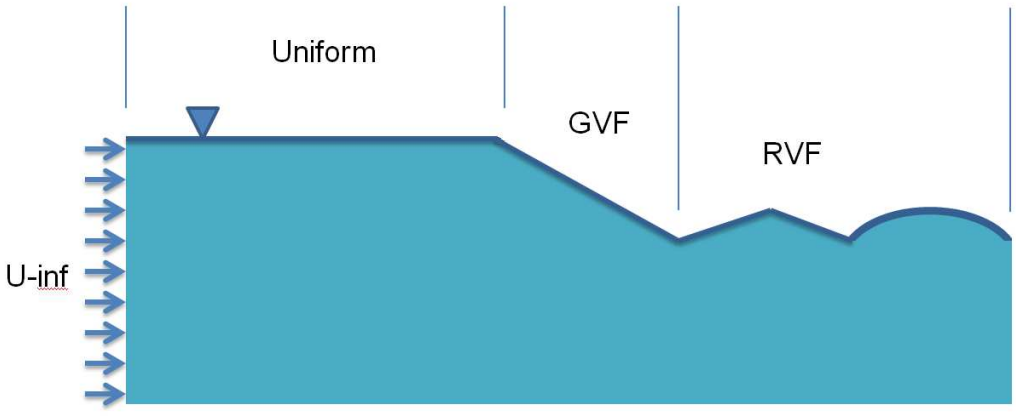

Figure 4-1 Open channel flow classifications that are separated according to region: uniform flow, gradually varying flow (GVF), and rapidly varying flow (RVF),

Table 4.1 Description of Froude Number

Froude Number	Physical Meaning of Ratio	Wave Travel Direction
Fr < 1.0	Wave Velocity > Velocity of Flow	Ripples would be able to propagate upstream and downstream
Fr = 1.0	Wave Velocity = Velocity of Flow	The velocity of ripples traveling upstream are equal to zero
Fr > 1.0	Wave Velocity < Velocity of Flow	Ripples would only be able to propagate downstream

consideration the critical depth (y_c) which is a parameter that can be considered an equivalent of the flow rate (Q). The critical depth is related to the total energy of the flow through another parameter known as the specific energy (E_s) of the flow. Every flow such as the one shown in Figure 4.2 has a total mechanical energy associated that is summed

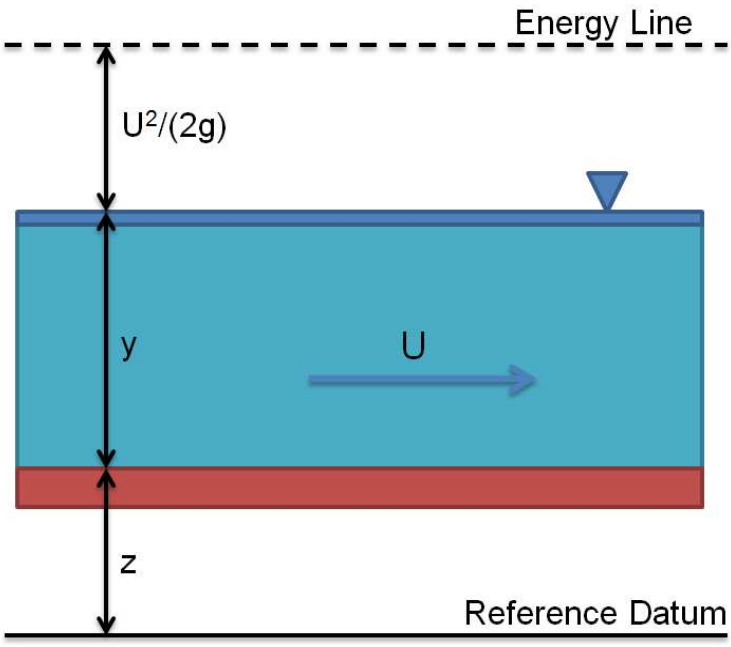

Figure 4.2 A schematic of the total mechanical energy contained in the flow.

as follows:

$$Total\ Energy = \left(\frac{U^2}{2g}\right) + (y) + (h) \tag{4.2}$$

$$= (Velocity\ Head) + (Pressure\ Head) + (Elevation\ Head)$$

If the reference datum is taken to be the bottom of the channel with z=0 then the specific energy (E_s) can be rewritten in terms of flow per unit width (q):

$$E_s = \frac{q^2}{y^2 2g} + y \tag{4.3}$$

Now with this equation for E_s we can plot specific energy against the pressure head, with Q held constant, which will produce a curve as shown in Figure 4-3.

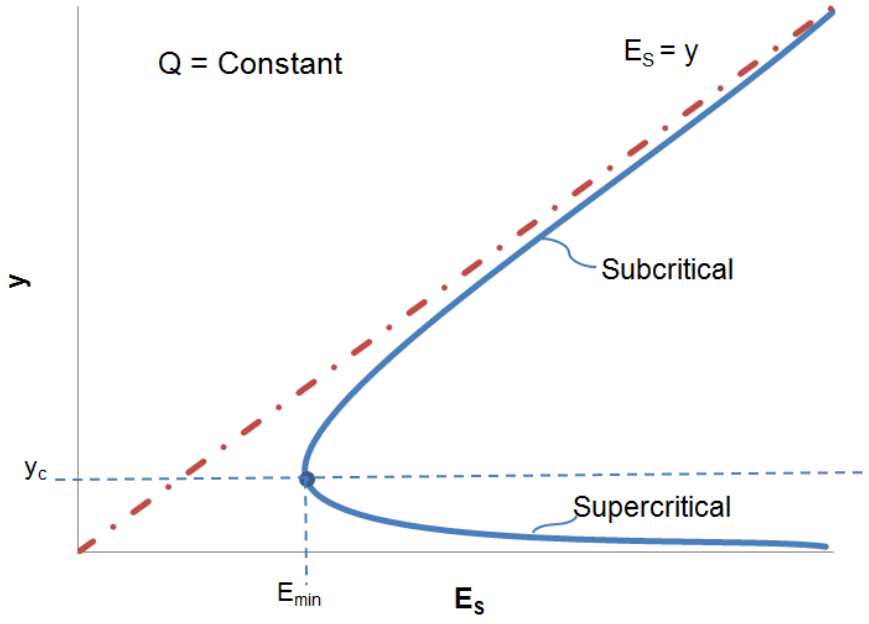

Figure 4.3 A plot of $y(E_s)$ with the flow rate Q held constant.

An equation for the critical depth (y_c) can be derived by substituting (U=Q/A) and setting the differential of E_s to zero:

$$E_s = \left(\frac{U^2}{2g}\right) + (y) = \frac{(Q/A)^2}{2g} + y \tag{4.4}$$

$$\frac{dE_s}{dy} = 0 = \left(\frac{(Q)^2}{2g}\frac{d}{dA}\left(\frac{1}{A^2}\right)\frac{dA}{dy}\right) + 1 \tag{4.5}$$

If the variables are specified for a critical depth, and since $\delta A = b\ \delta y$ for area (A) ; in the limit $b = dA/dy$ then the result is:

$$0 = 1 - \frac{Q^2}{2g}(b_c)\left(2\frac{1}{A_c^3}\right) \tag{4.6}$$

$$\frac{Q^2(b_c)}{gA_c^3} = 1 \tag{4.7}$$

Substituting $Q = qb$ and $A_c = b_c y_c$, this equation then can be solved for critical depth as follows:

$$y_c = \left(\frac{q^2}{g}\right)^{1/3} \tag{4.8}$$

Now from Figure 4.3 it is clear that two important rules apply for a constant flow rate:

1. The minimum value E_{min} occurs at the critical depth.
2. For all other values of E_s there are two possible flow depths where one is subcritical and the other is supercritical.

4.4 Grid Refinement Study

Several simulations were run to determine the time it would take for most simulations to reach a steady state. It was found that a steady state could be observed in most tests if the simulation was advanced to time t=800 seconds. In the VOF method the computational domain mesh can be composed of non-uniform grid cells such as shown in Figure 4.4. The current version of the CLSVOF code requires that a square grid be used

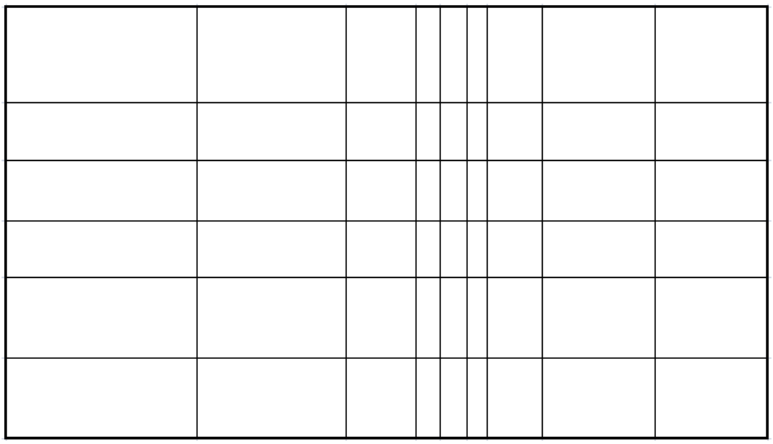

Figure 4.4 An example of a non-uniform mesh.

for the simulation. A grid refinement study was necessary to determine the appropriate grid cell size to use for each test. A series of five simulations with increasing grid cell size was completed to evaluate the most appropriate grid cell size. The results of the testing are shown in Figure 4.5. The regional area of interest for this study is the free surface above the step from x/h_0 =13 to x/h_0 = 23 for most simulations so it is clear from Figure 4.5 that for each simulation the grid cell size will not matter in the overall profile. A grid cell size of 8.083 is selected to use for analysis in the simulations of this study. A zoomed in graph of the free surface from x/h_0 =20.0 to x/h_0 = 20.5 is shown which shows that for the selected grid cell size the profile of the free surface will only vary by $y/h_0 \sim \pm$ .01. This tolerance is within an acceptable range for an accurate study of the free surface.

4.5 Preliminary Testing of Numerical Model

As has been mentioned before, careful specification of the parameters and range of testing is recommended in order to ensure accurate results. If the Froude number is written in terms of the initial free surface (h_0) and inlet velocity (U_{-inf}) then Equation 4.1

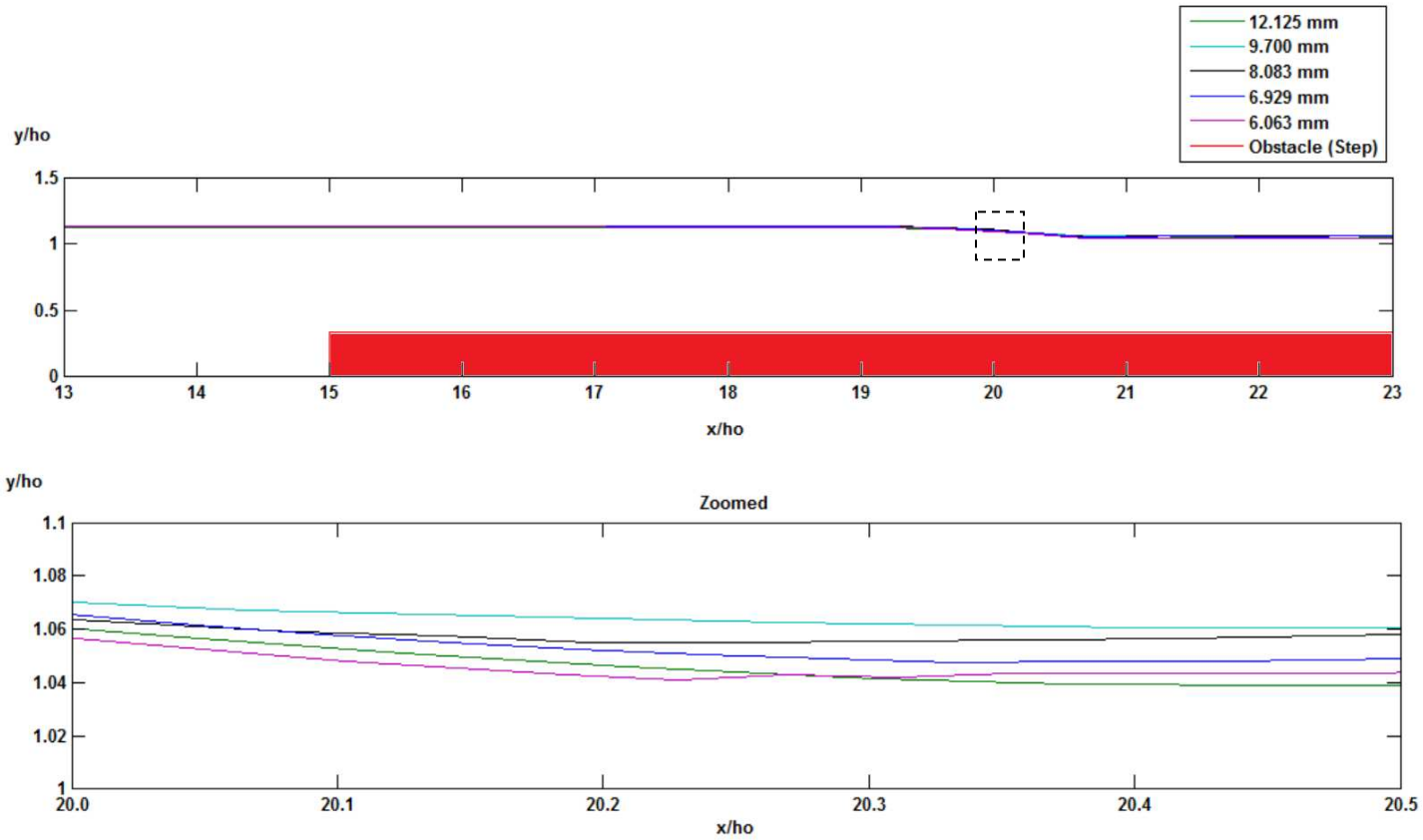

Figure 4.5 Testing of the grid cell size for numerical simulations. A plot of the free surfaces generated for each cell size is shown in the zoomed view.

becomes:

$$Fr_0 = \frac{(U_{-inf})}{\sqrt{gh_0}} \tag{4.9}$$

where Fr_0 is the Froude number taken at time t=0 when free surface is at a height of h_0 and is equivalent to the incident flow velocity of [2]. It has been shown in [2] that as the incident flow velocity increases the pressure head will also increase in response. This is primarily the reason the boundary conditions at the inlet will tend to cause problems for flows with a high incident flow velocity. It is because of this that testing of the flow will be limited to flows with Fr_0 <0.5 where the pressure head does not increase significantly enough to affect the accuracy. The dimensions of the testing will be another factor that allows for the boundary conditons at the inlet to not impair the accuracy of the flow simulation. The length of the computational domain is nearly 35 times the height of the flow, and the actual scaling is shown in Figure 4.6. It is assumed that at steady state with this scaling there is enough distance from the osbtacle that the numerical accuracy is maintained for flows with $Fr_0 < 0.5$.

A preliminary test simulation was performed for a step height (B/h_0) = 0.3333 at different values of Fr_0 to see whether the pressure head was affected by the boundary conditions. The results are plotted in Figure 4.7, and are in good agreement with the results presented in [2]. It is clear that the tested range chosen for the flow is acceptable. The testing will be for a stream gradient that is a downhill slope which is another reason that the boundary conditions at the inlet will not have a negative impact on the simulation. It can be seen from Figure 4.8 that for our geometry a downhill slope will tend to cause

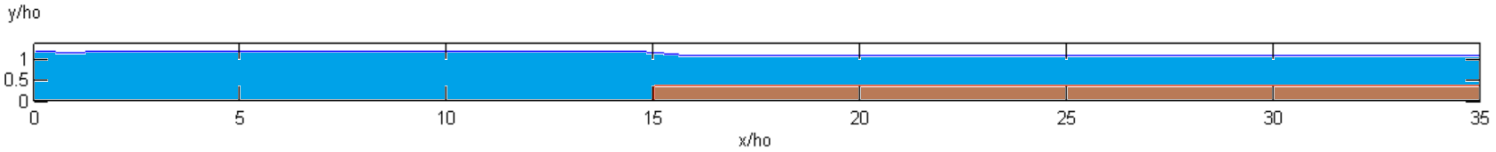

Figure 4.6 A full scale plot of the whole computational domain.

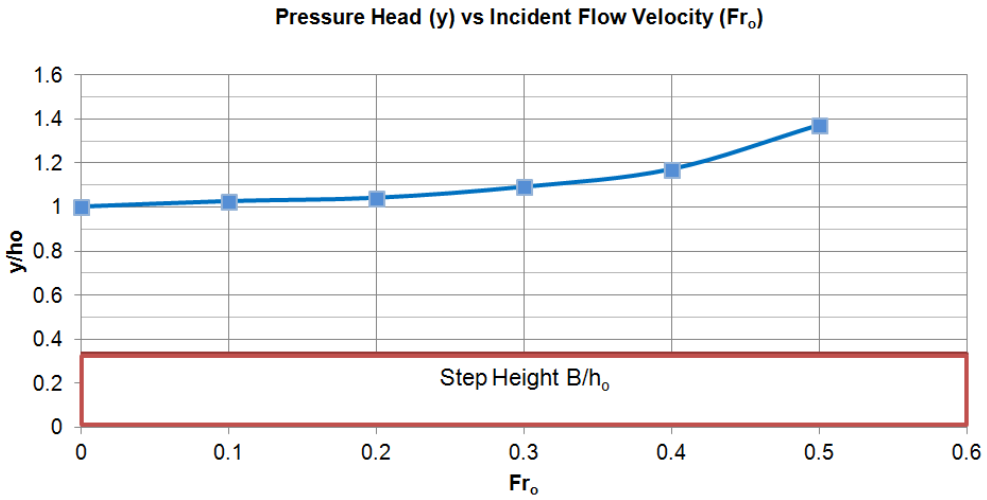

Figure 4.7 Dependence of the pressure head on the incident flow velocity for a step height of 0.3333.

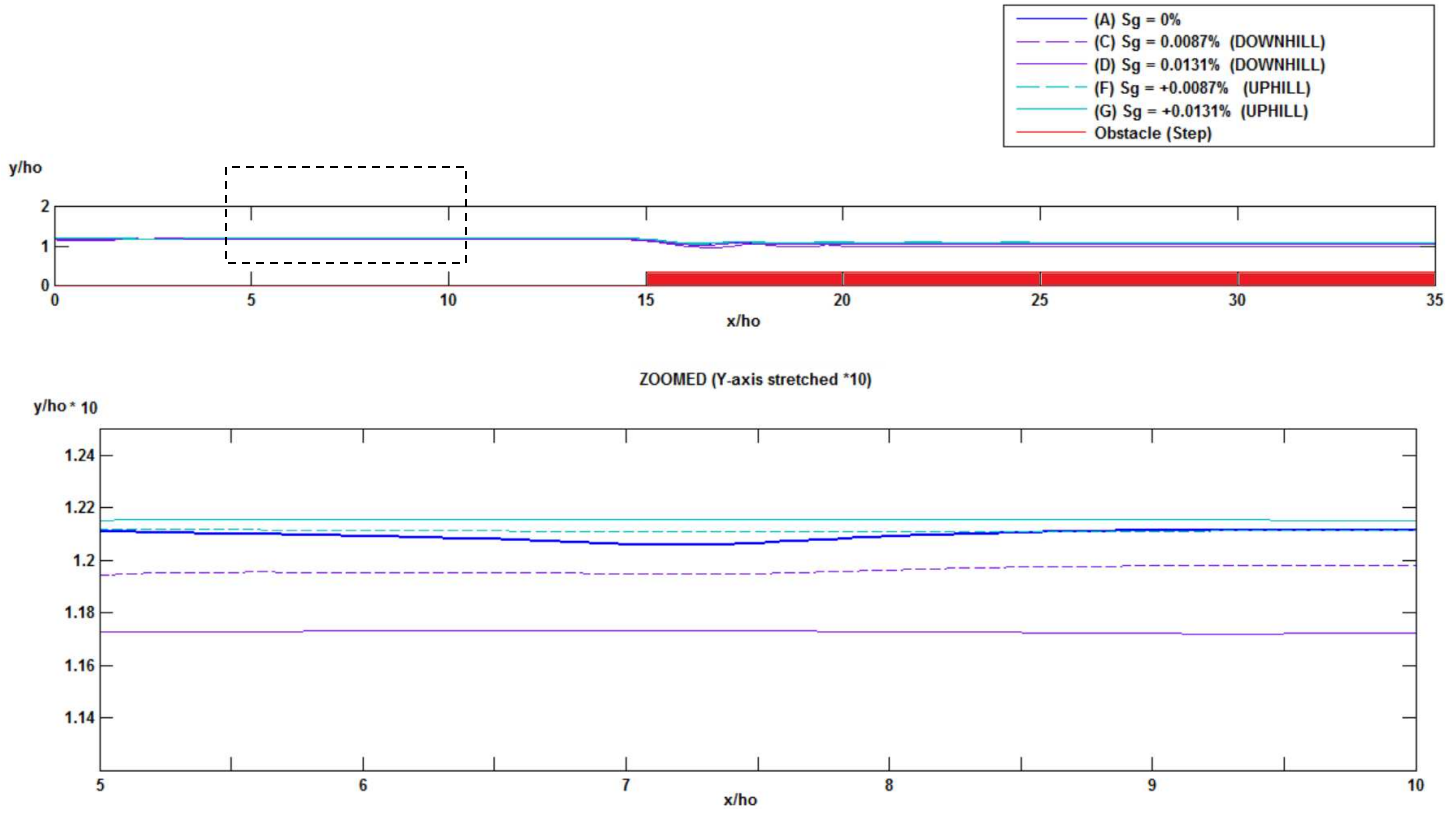

Figure 4.8 A zoomed graph of the free surface profile with the y-axis stretched by ten times (*10). The profiles show the trend for downhill and uphill Sg.

the depth of the free surface near the inlet to decrease while an uphill slope will cause an increase. It is because of this effect that the accuracy of downhill testing will be maintained. A full scale graph of the entire free surface of the flow is shown for reference in Figure 4.8.

4.5.1 Comparison of Numerical Results to Experimental Results

A numerical analysis was done to compare the numerical model used with the experimental data that is available to determine the range of accuracy that can be expected. It is necessary to first rearrange Equation 4.9 before taking a look at the results in order to put it in a more relevant form. The equation for critical depth can be rearranged into a dimensionless form by first introducing the term $\sqrt{g}$ as follows:

$$y_c = \left(\frac{q^2}{g}\right)^{1/3} = \left[\frac{q}{\sqrt{g}}\right]^{\frac{2}{3}} \tag{4.10}$$

Then by swapping the radical to the left hand side of the equation and multiplying by $(h_0)^{\frac{3}{2}}$ on both sides of the equation will result in:

$$y_c{}^{\frac{3}{2}} = \left[\frac{q}{\sqrt{g}}\right]\left(\frac{h_0}{h_0}\right)^{\frac{3}{2}} \tag{4.11}$$

This form can be rearranged to make the critical depth a function of incident flow velocity and the calculated value of pressure head (y) which results in:

$$\frac{y_c}{h_0} = \left[\frac{q}{\sqrt{g h_0}\,(h_0)}\right]^{\frac{2}{3}} = \left[\left(\frac{y}{h_0}\right)(Fr_0)\right]^{\frac{2}{3}} \tag{4.12}$$

The term y_c is physically the critical depth behind a step in a channel with a horizontal stream bed so to indicate this y_c is redefined as y_* which results in a final form of:

$$\frac{y_*}{h_0} = \left[\left(\frac{y}{h_0}\right)(Fr_0)\right]^{\frac{2}{3}} \tag{4.13}$$

The plot of the free surface that was constructed using the CLSVOF method is shown in Figure 4.9 for y_*=74.5mm. The plot is in good agreement with the experimental data of [1], and shows a slight improvement on the estimation of the pressure head.

4.6 Range of Testing

The range of testing was divided into three series of simulations in order to study the effect of the stream gradient, incident flow velocity, and step height on the flow. The first parametric study was focused on the effect of the change in stream gradient on the free surface. To observe this several low and moderate stream gradient flows were simulated for three different incident flow velocities. Table 4.2 lists each test that was performed for this first range of simulations. The next series of tests studied the effect that a change in the incident flow velocity would have for low and moderate stream gradient values. They are summarized in Table 4.3. These simulations were also performed to correlate the effect a stream gradient has on the pressure head as the incident flow velocity is increased. The final series of tests are shown in Table 4.4 which examined the effect that an increase in step size has on the free surface for an increasing downhill stream gradient.

4.7 Stream Gradient Testing

The results of the low and moderate stream gradient testing for a channel flow with Fr_0 = 0.35 are shown Figure 4.10 and Figure 4.11. The free surface profile in the region above the obstacle shifts quickly from a RVF to a GVF profile when a very small stream gradient is applied to the channel. It can be seen from the moderate stream gradient test results that an increase in slope will cause a decrease in the pressure head. The pressure head at this incident flow velocity drops very quickly from Sg = 2.094% to Sg = 2.443%; at Sg = 3.142% the pressure head has almost been reduced to the height of the step. The low stream gradient testing for a flow with Fr_0 = .40 is shown in

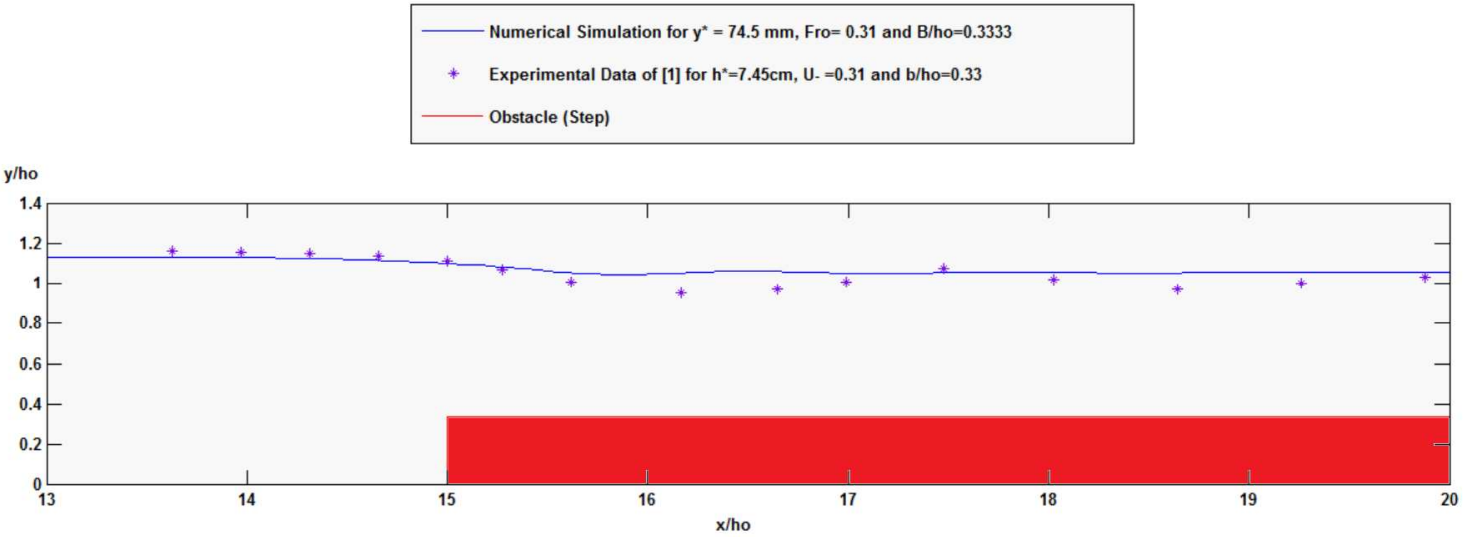

Figure 4.9 The steady state free surface profile for y* = 74.5 mm and the experimental data for h* = 7.45 cm.

Table 4.2 Low and moderate stream gradient tests.

Fr_O = .35		Fr_O = .40		Fr_O = .45	
Low Sg	Moderate Sg	Low Sg	Moderate Sg	Low Sg	Moderate Sg
0%	1.745%	0%	1.745%	0%	1.745%
0.175%	2.094%	0.175%	2.094%	0.175%	2.094%
0.349%	2.443%	0.349%	2.443%	0.349%	2.443%
0.524%	3.142%	0.524%	3.142%	0.524%	3.142%
0.698%		0.698%		0.698%	
0.873%		0.873%		0.873%	

Table 4.3 Incident flow velocity tests for Fro =0.1 to 0.5

Sg		
0%	0.524%	2.443%
Fr_O	Fr_O	Fr_O
0.1	0.1	0.1
0.2	0.2	0.2
0.3	0.3	0.3
0.4	0.4	0.4
0.5	0.5	0.5

Table 4.4 Step height testing for low and moderate Sg

Sg		
0%	0.524%	2.443%
B/h_O	B/h_O	B/h_O
0.222	0.222	0.222
0.278	0.278	0.278
0.389	0.389	0.389
0.500	0.500	0.500

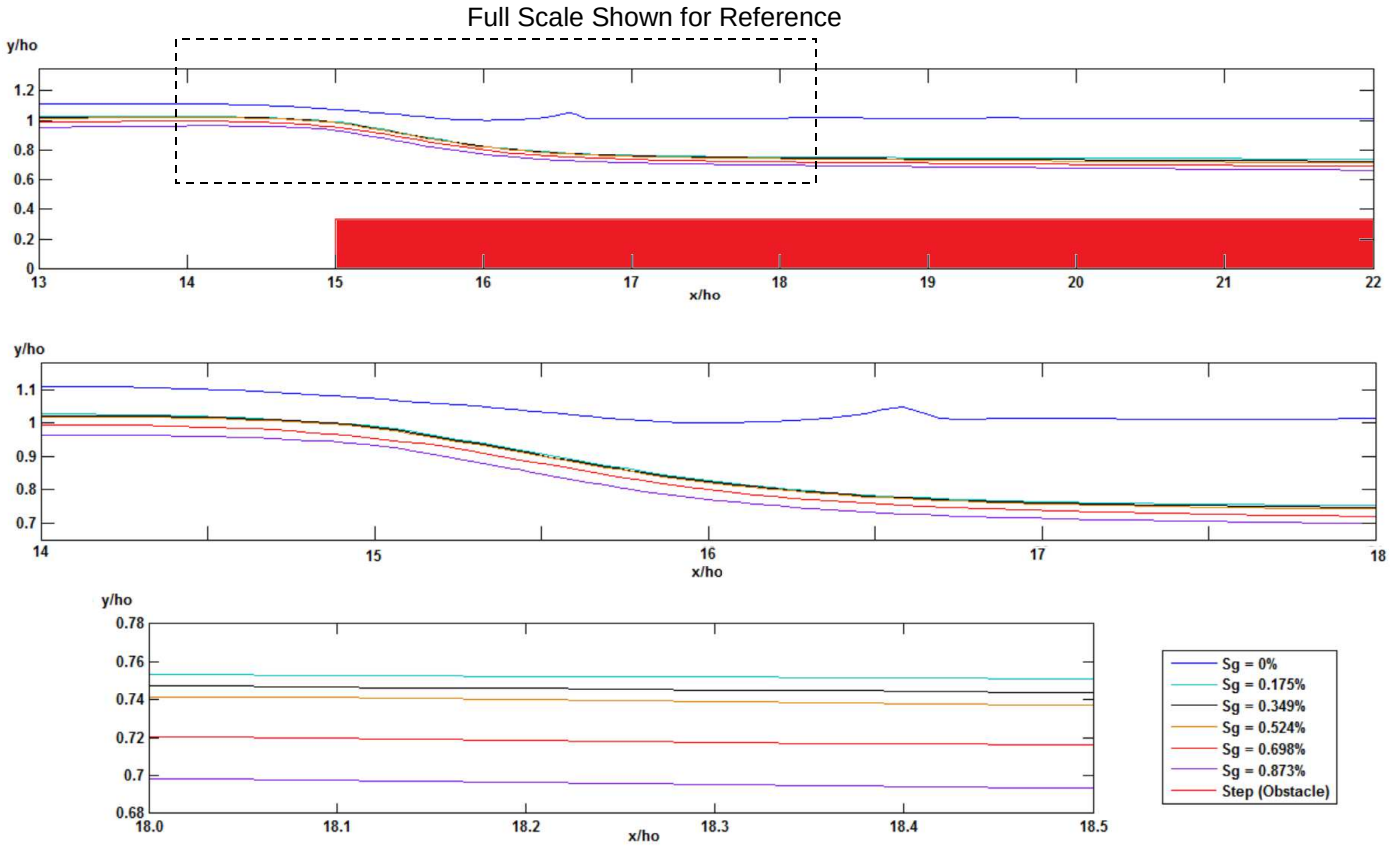

Figure 4.10 The low stream gradient testing for Fr_O = .35

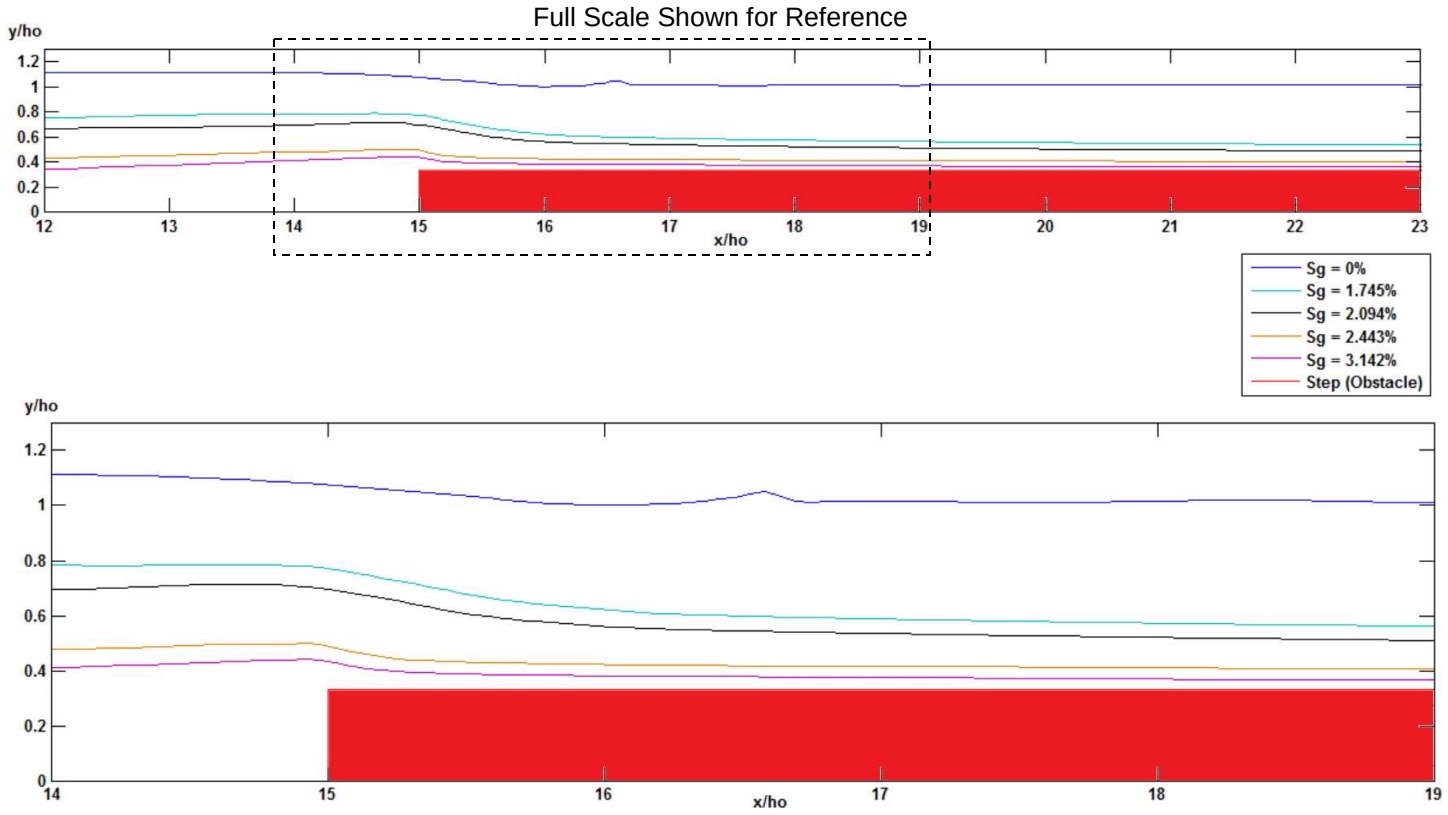

Figure 4.11 The moderate stream gradient testing for Fr_O = .35.

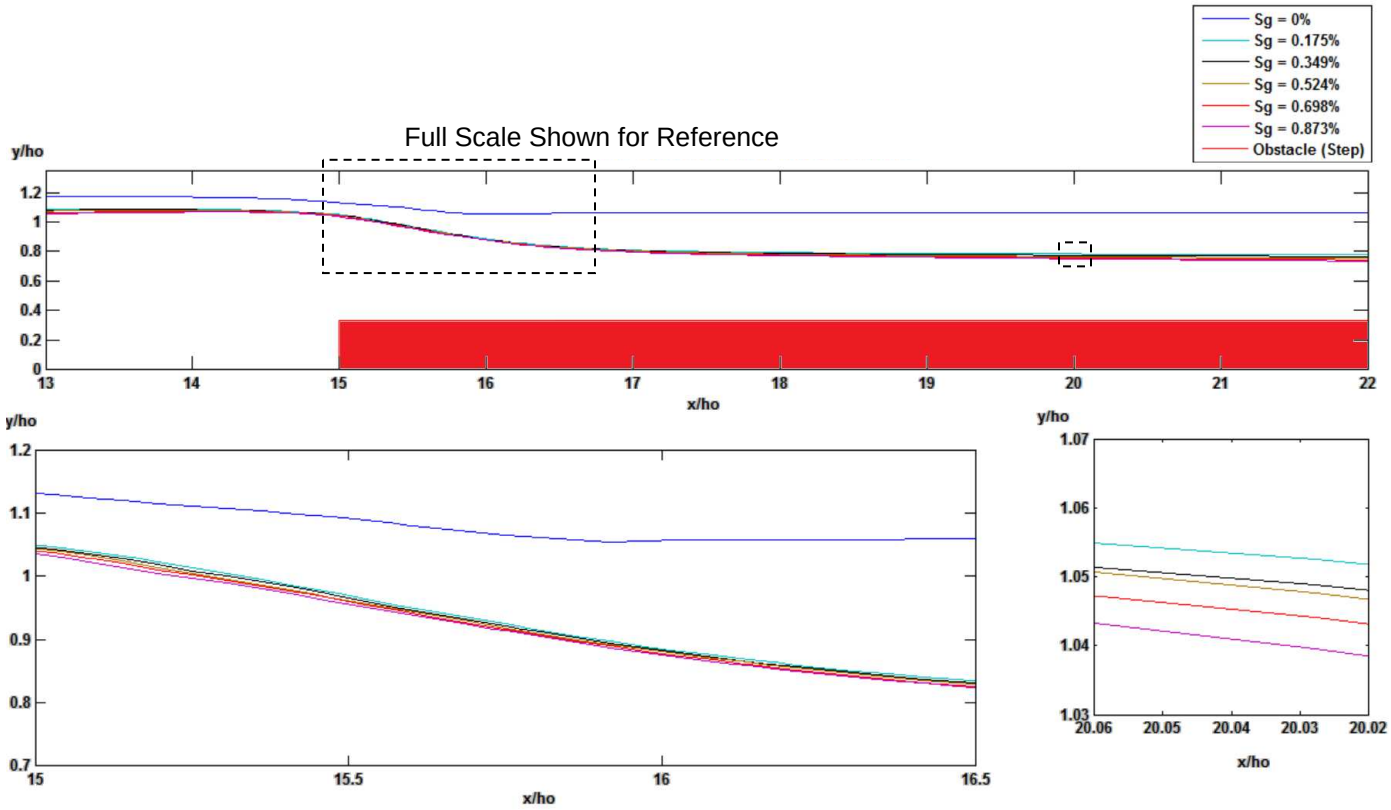

Figure 4.12 The low stream gradient testing for Fr_O = .40.

Figure 4.12. As the stream gradient is increased there is not much change in the height of the free surface that can be seen. The initial drop in free surface height as Sg = 0% is increased to Sg = 1.175% for the region between x/h_0 = 15.0 to x/h_0 = 20.0 is still very much the same as in the low gradient tests for Fr_0 = .35. The moderate stream gradient testing for Fr_0 = .40 is shown in Figure 4.13 with the free surface profiles much more evenly spaced out. The low and moderate stream gradient test results for Fr_0 = .45 are shown in Figure 4.14 and Figure 4.15. An interesting change in the profile occurs from x/h_0 =19.0 to x/h_0 = 22.0 in the low stream gradient testing for Sg = 0.175% where an undulation appears in the free surface.

The pressure head was measured for each simulation at x/h_0 = 5.0 before the flow encounters the obstacle and is plotted against the stream gradient in Figure 4.16. The drop in pressure head is very minimal for the low gradient below Sg = 1.0%, but as the stream gradient shifts into a moderate gradient the drop in pressure head begins to change very quickly. In the region between Sg = 2.50% and Sg = 3.50% the pressure head is reduced below the height of the step. The minimum height (Hmin) of the free surface for each simulation was plotted in Figure 4.17 to show the trend as the stream gradient is increased. The trend reflects the drop in pressure head very well and the relation is clearly shown in both figures.

4.8 Incident Flow Velocity Testing

The incident flow velocity testing began with a series of tests from Sg = 0% with increasing incident flow velocity from Fr_O = 0.10 to Fr_O = 0.50. The results of that series of testing are shown in Figure 4.18. The next series of tests were run with the same incident flow velocities but at Sg = 0.524%. The results of that set of incident flow velocity testing are shown in Figure 4.19.The effect of even a small stream gradient is seen right away as a significant shift in the free surface profiles can be seen as the incident flow

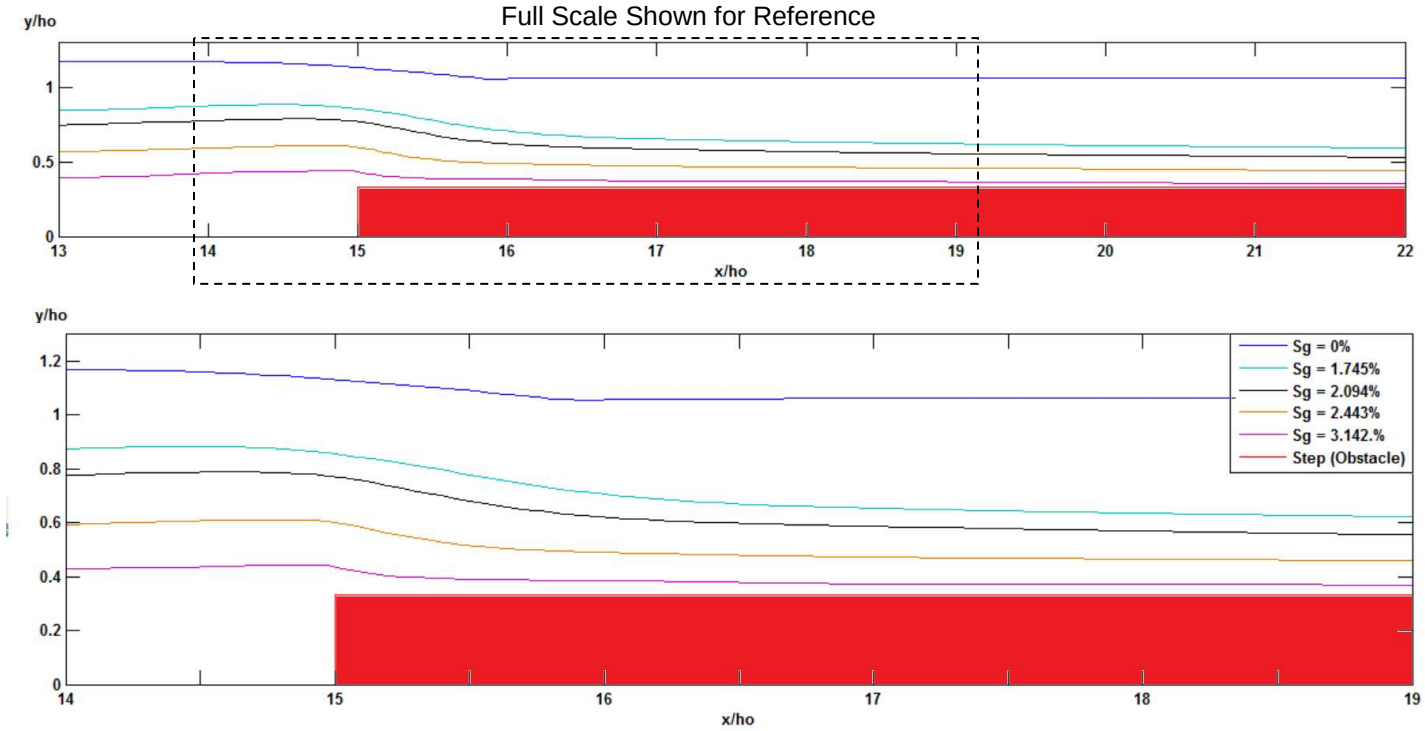

Figure 4.13 The moderate stream gradient testing for Fr_O = .40.

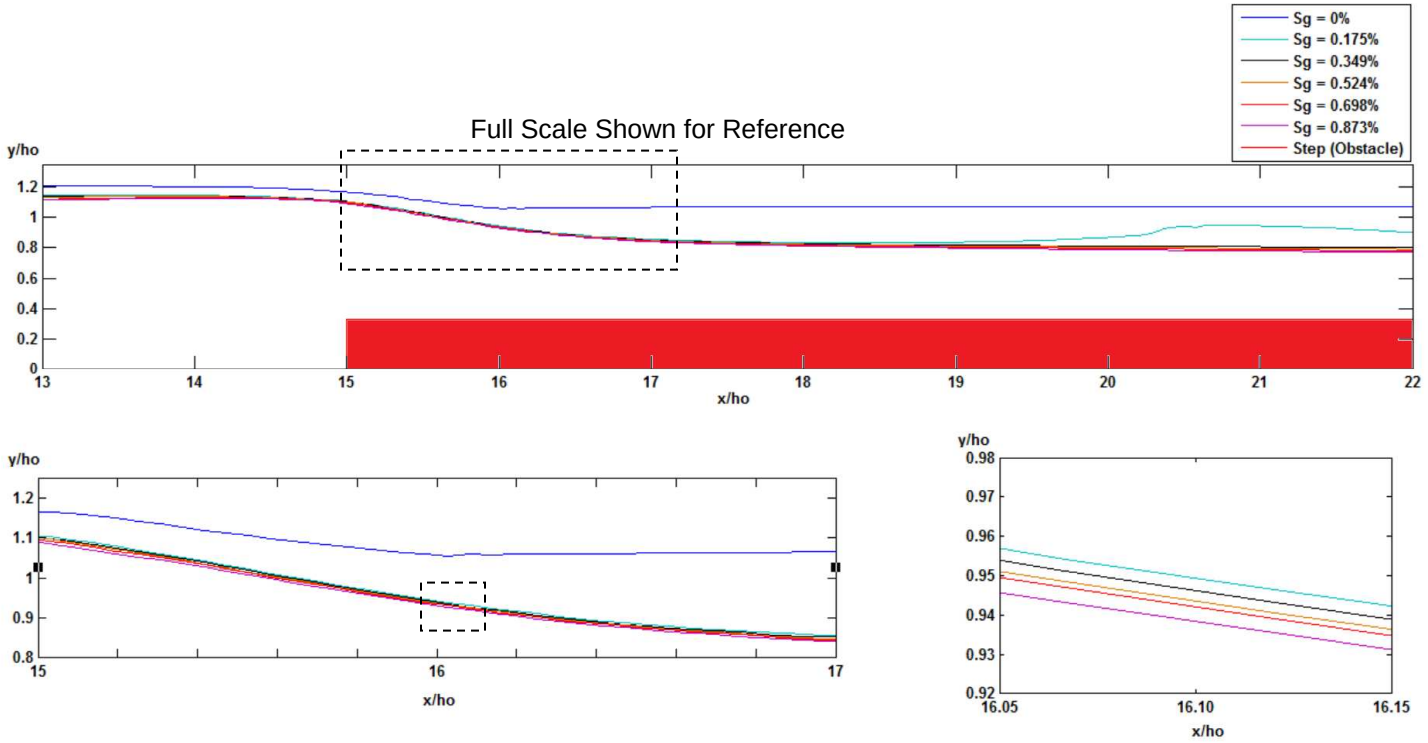

Figure 4.14 The low stream gradient testing for Fr_O = .45.

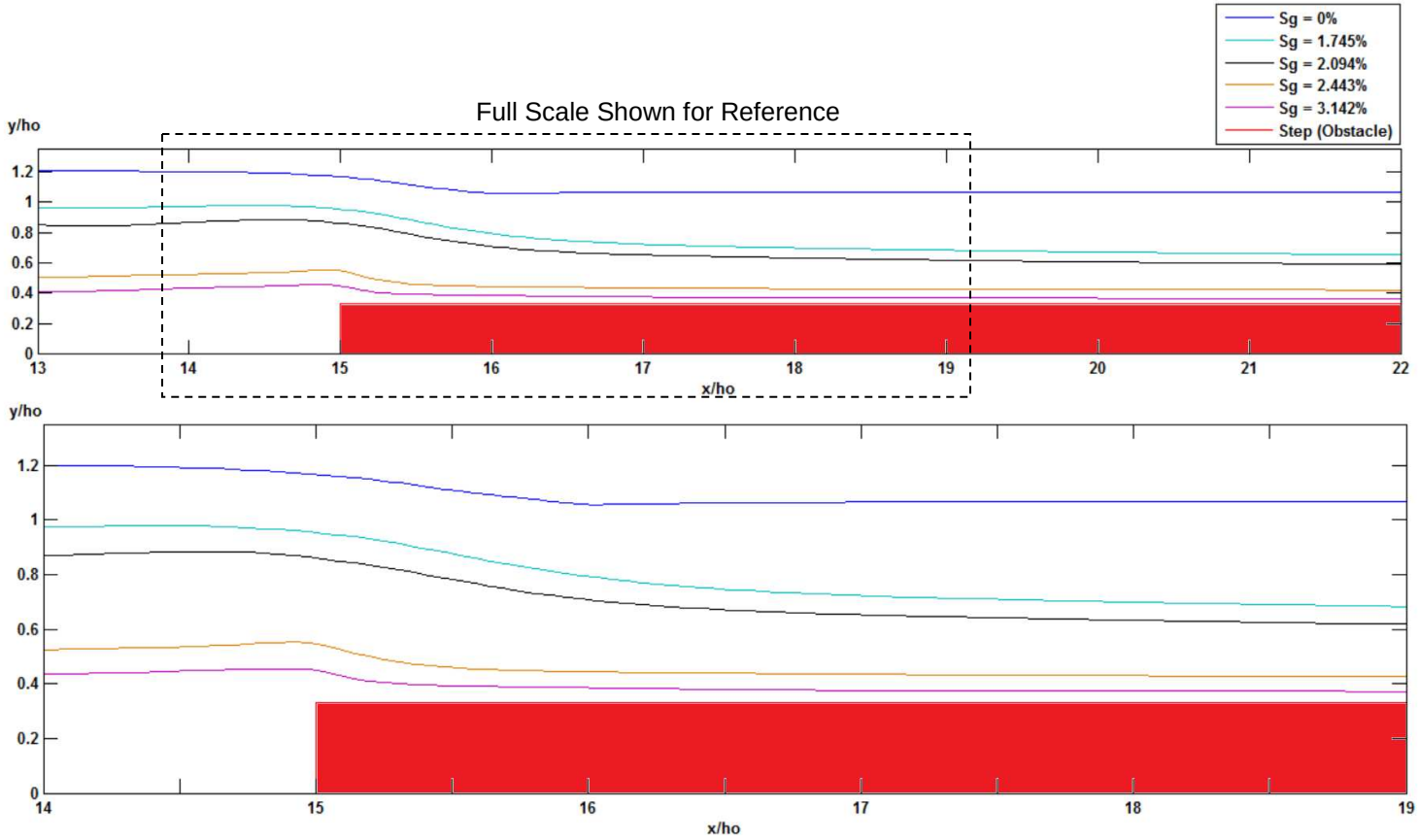

Figure 4.15 The moderate stream gradient testing for Fr_O = .45.

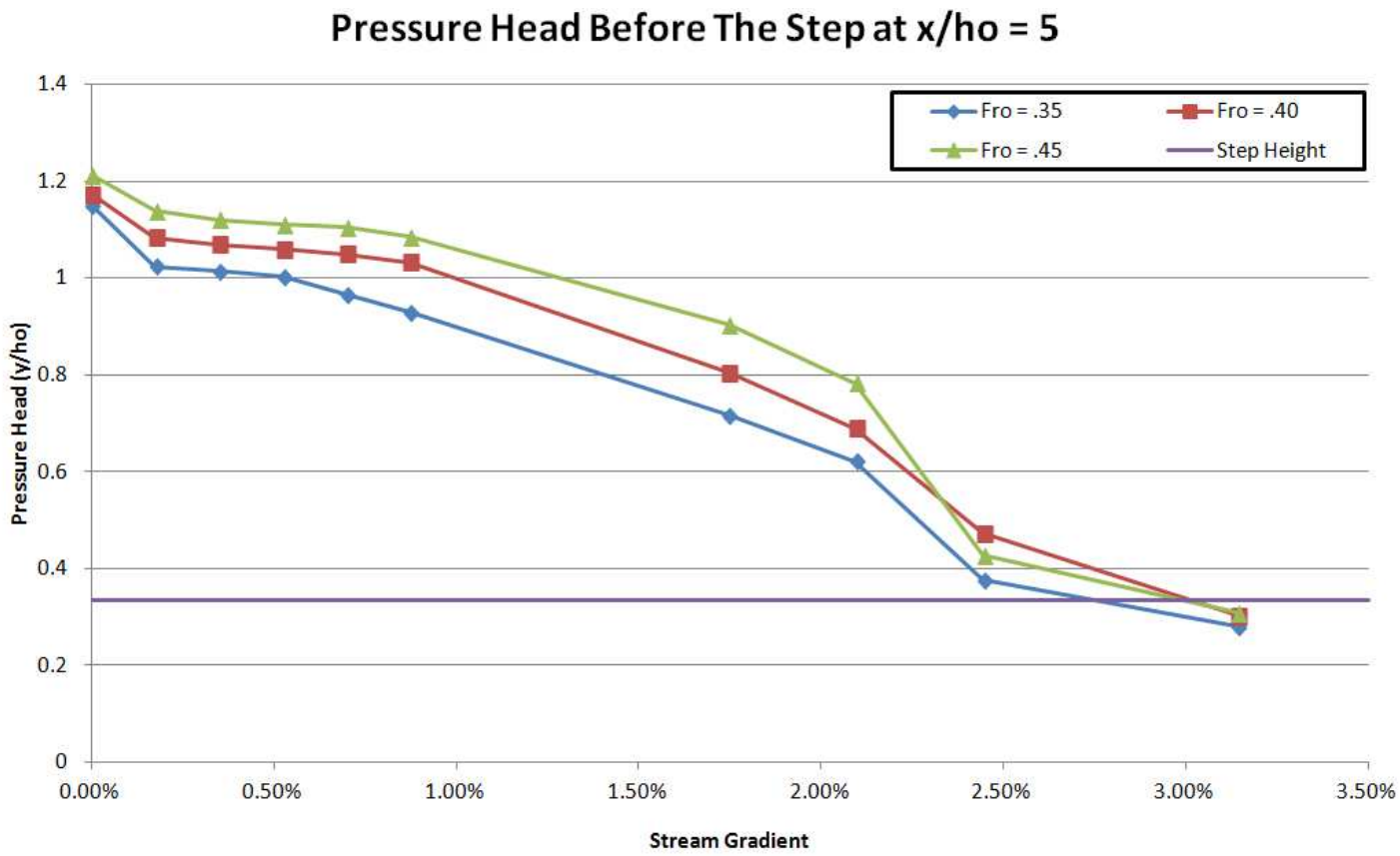

Figure 4.16 A Graph of the Dependence on Stream Gradient for the Pressure Head.

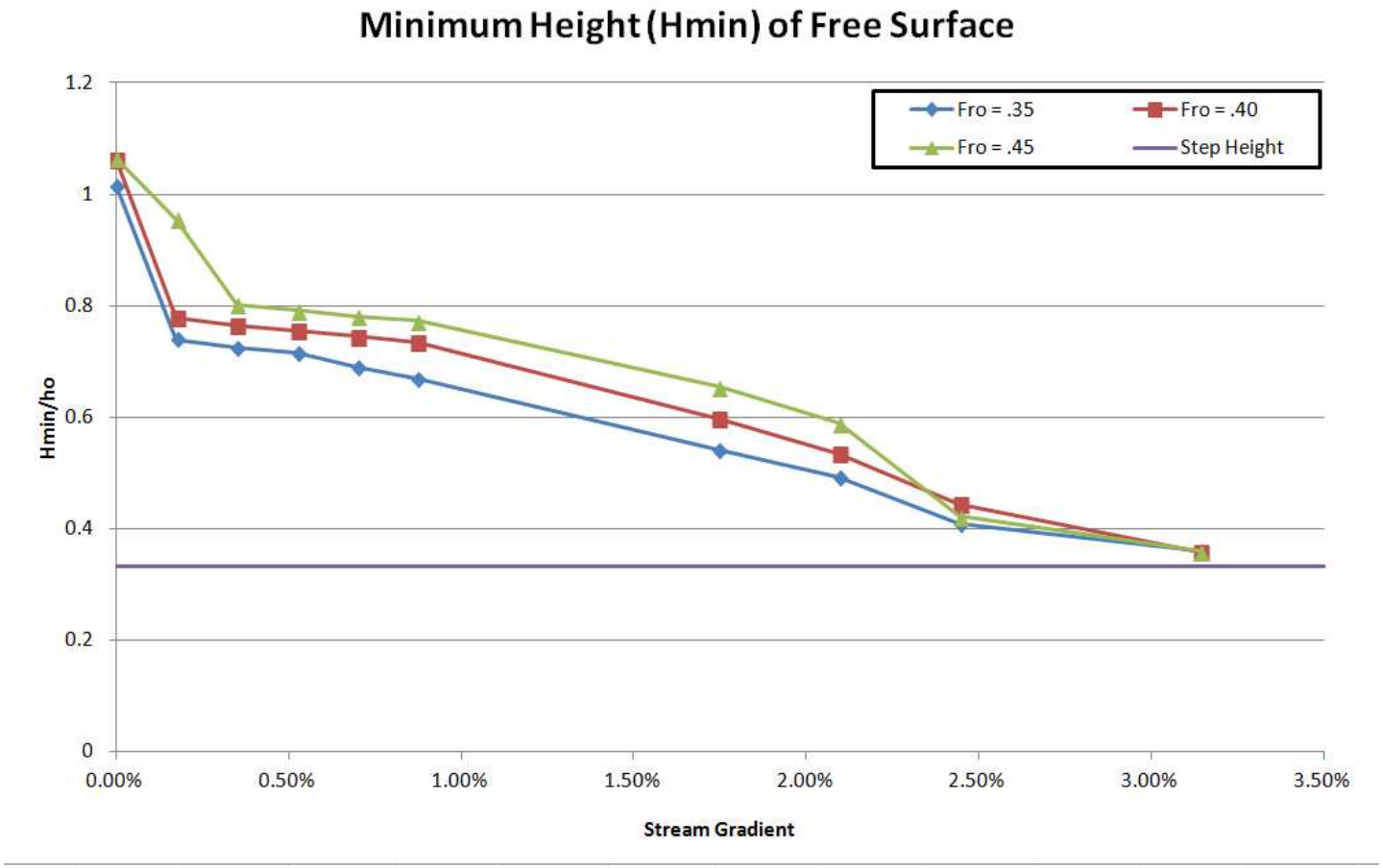

Figure 4.17 A Graph of the Dependence on Stream Gradient for the Minimum Height (Hmin).

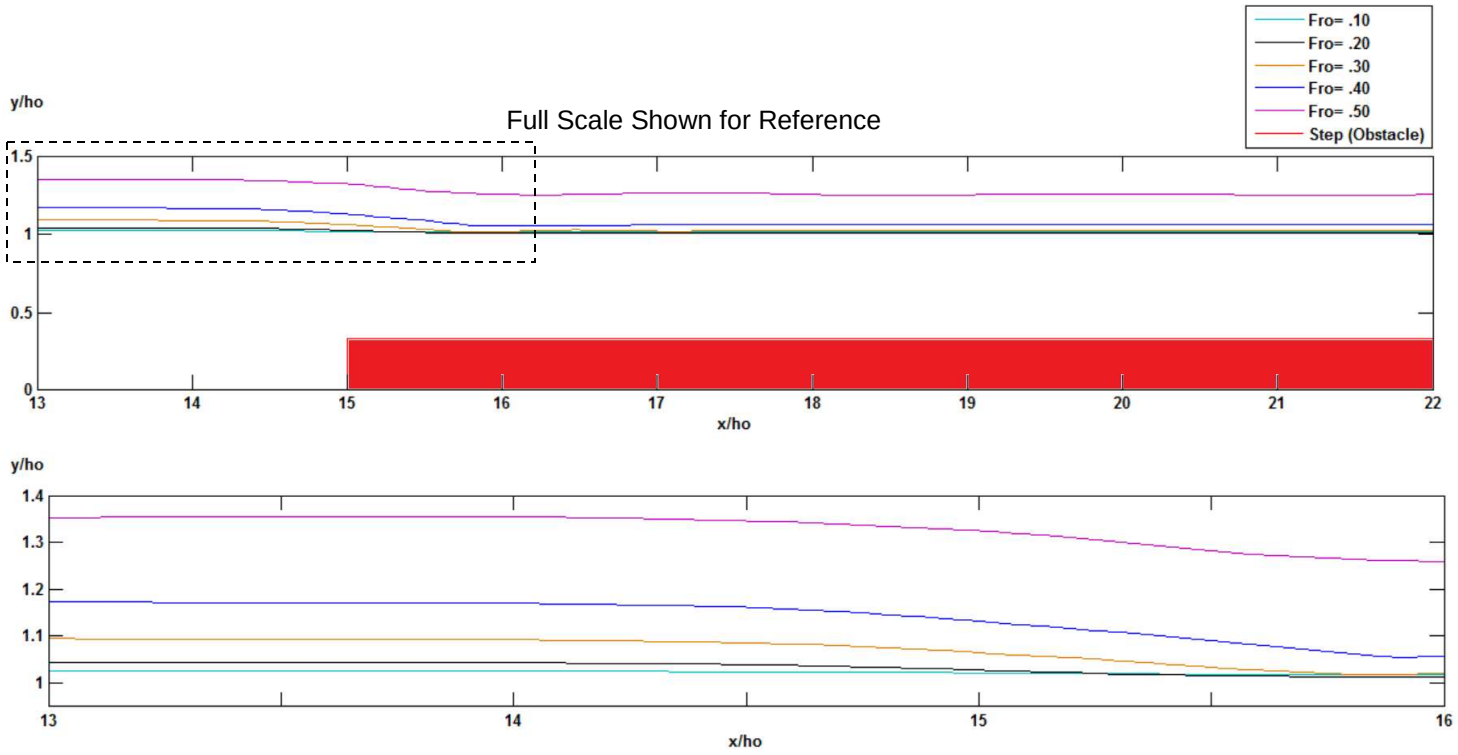

Figure 4.18 The incident flow velocity testing results for Sg=0%.

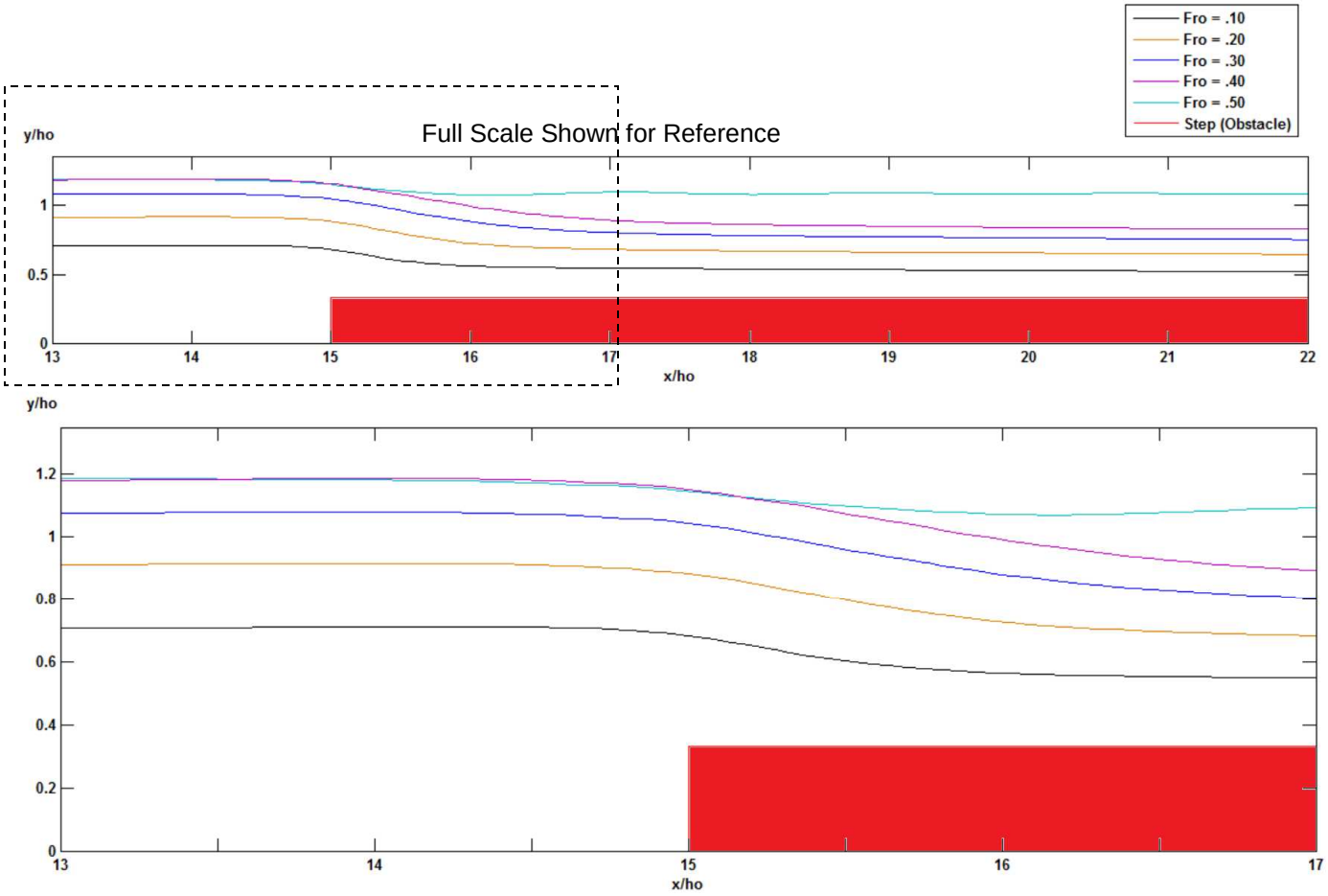

Figure 4.19 The incident flow velocity testing results for Sg=0.524%.

velocity is increased. The final set of testing was done for Sg = 2.443%, and is shown in Figure 4.20. In the case of a moderate stream gradient it can be seen that the free surface profiles are spread out more evenly as the incident flow velocity is increased.

4.9 Step Height Testing

The next phase of testing began with a series of simulations that were run at a constant incident flow velocity with Fr_O = .45 and Sg = 0% for a range of step heights. The results for this testing are shown in Figure 4.21. The same set of simulations were then performed only this time for a steam gradient of 0.524%. The results of these simulations are depicted in Figure 4.22 and there is a change in the free surface that occurs in the region between x/h_0 =15.0 and x/h_0 = 19.0 as the step height is increased. The small undulation that appears in the free surface for B/h_0 = 0.500 in the low gradient is smoothed out evenly along with the other profiles. Another set of simulations were then performed for a moderate stream gradient of 2.443%, and the results are shown in Figure 4.23. The profiles for B/h_0 = 0.278 and B/h_0 = 0.389 begin to spread apart, and a more significant drop in the pressure head can be noticed.

4.10 Critical Depth Analysis

The critical depths for Fr_0 = 0.35, 40, and 45 are plotted against the minimum height (Hmin) of the free surface and the pressure head (y) to observe when the flow will drop below the y*/ho. Figure 4.24 is the plot of the dependence of(y) and Hmin on the stream gradient for Fr_0 = 0.35, and also shows the critical depth of $y*/h_0$ = 0.545. It is shown in the figure when the minimum height and the pressure head drop below the critical depth with the dashed lines. Figure 4.25 is for Fr_0 = 0.40 and shows the critical depth for $y*/h_0$ = 0.604. When the incident flow velocity is increased to 0.40 the point at which minimum height crosses the critical depth occurs at a slightly lower stream gradient. Figure 4.26 is for Fr_0 = 0.45 and shows the critical depth for $y*/h_0$ = 0.667.

Once again, it can be seen that the point at which Hmin crosses the critical depth occurs at a slightly lower stream gradient. It can thus be interpreted that as the incident flow velocity is increased the stream gradient will become more significant since the critical depth will be reached sooner.

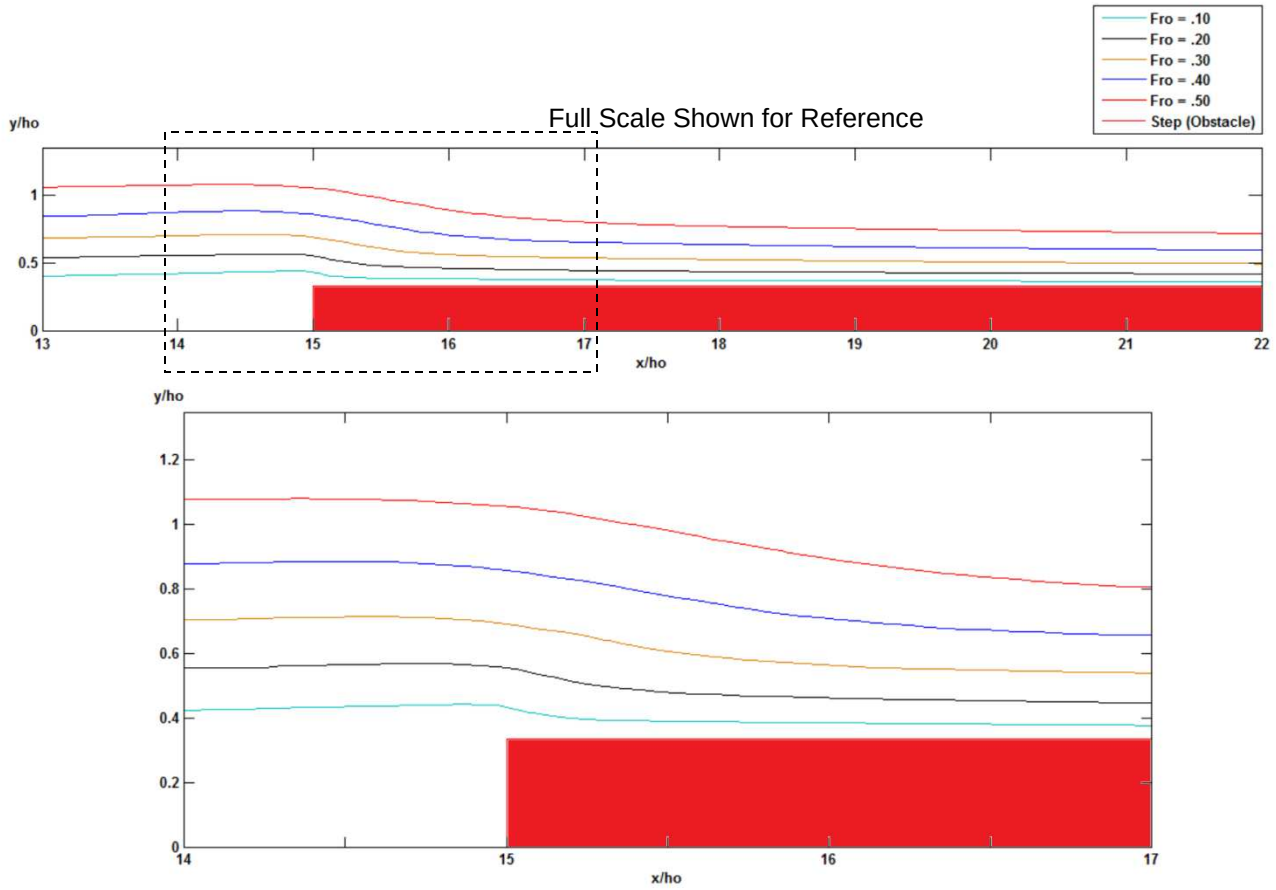

Figure 4.20 The incident flow velocity testing results for Sg=2.443%.

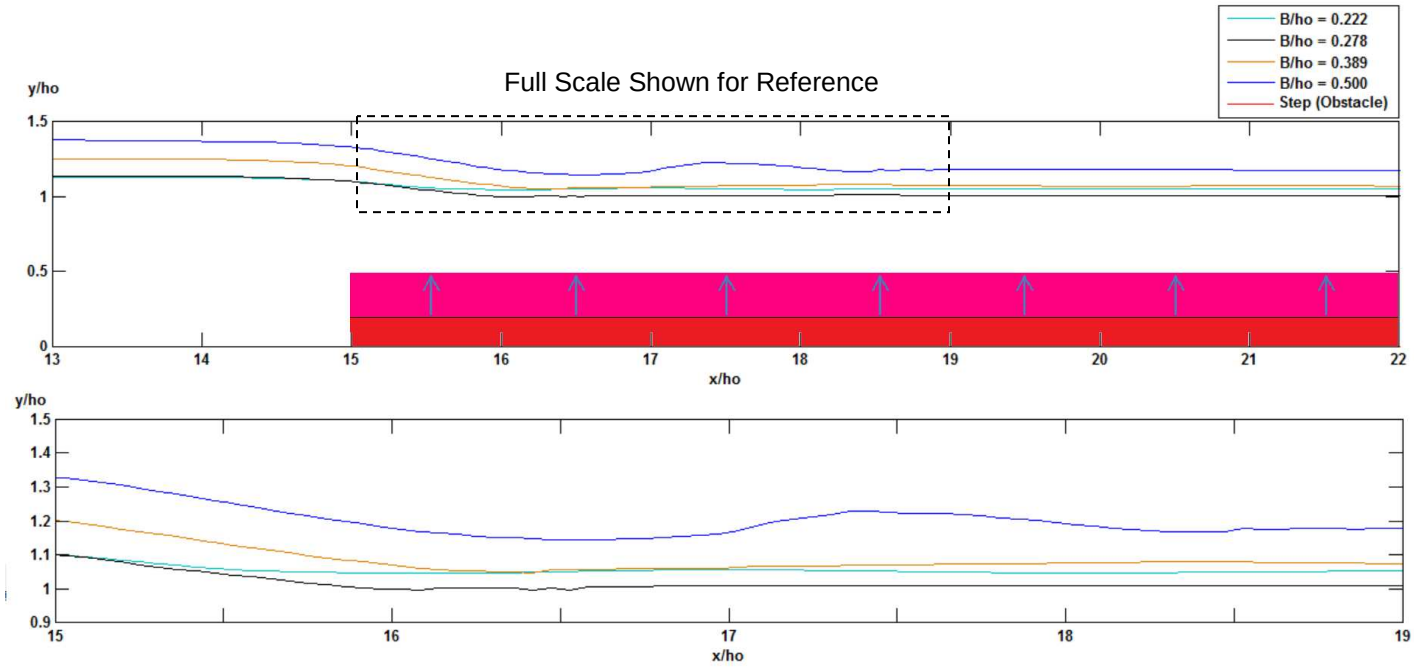

Figure 4.21 Testing results for a Sg = 0% and Fr_O = .45 with increasing step height.

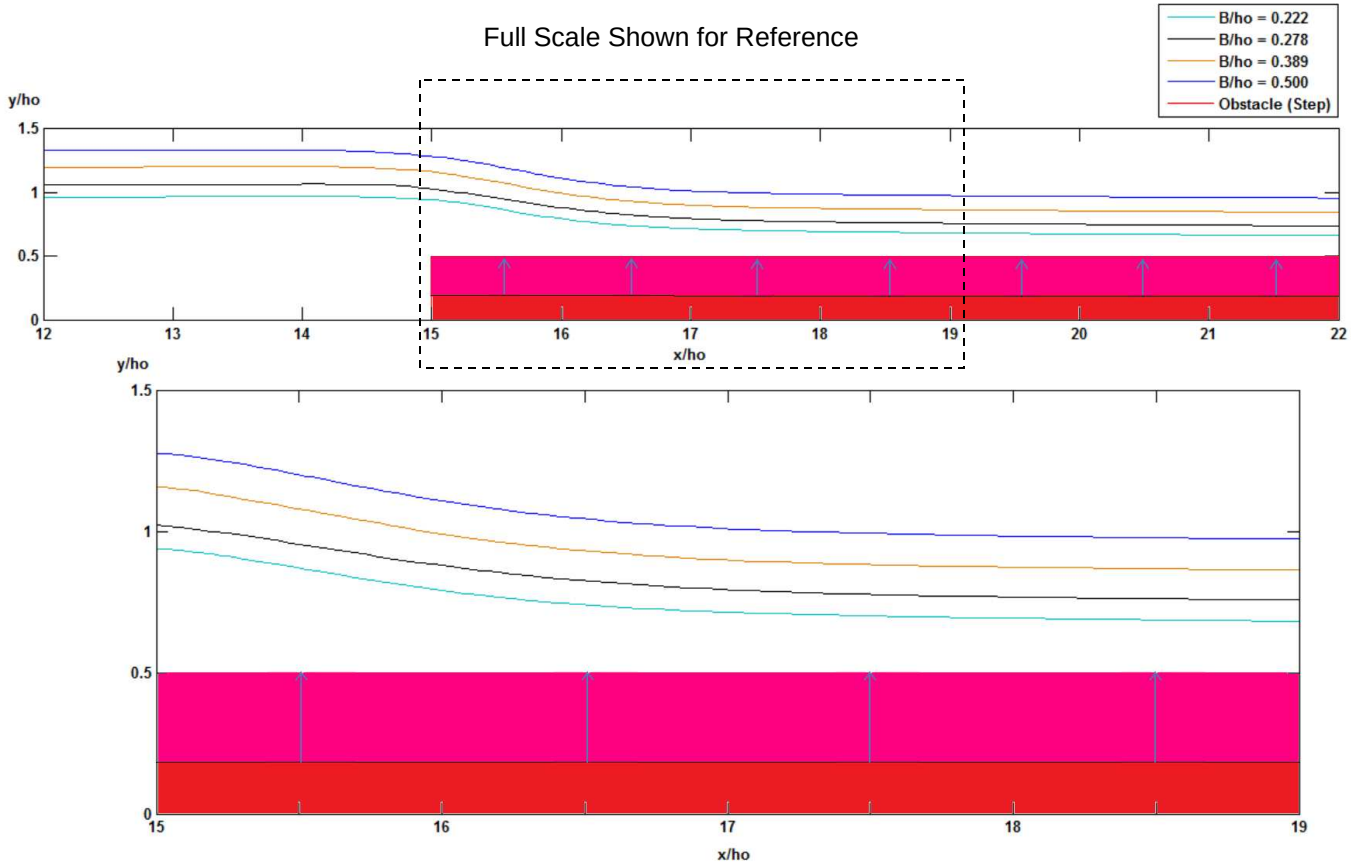

Figure 4.22 Testing results for a Sg = 0.524% and Fr_O = .45 with increasing step height.

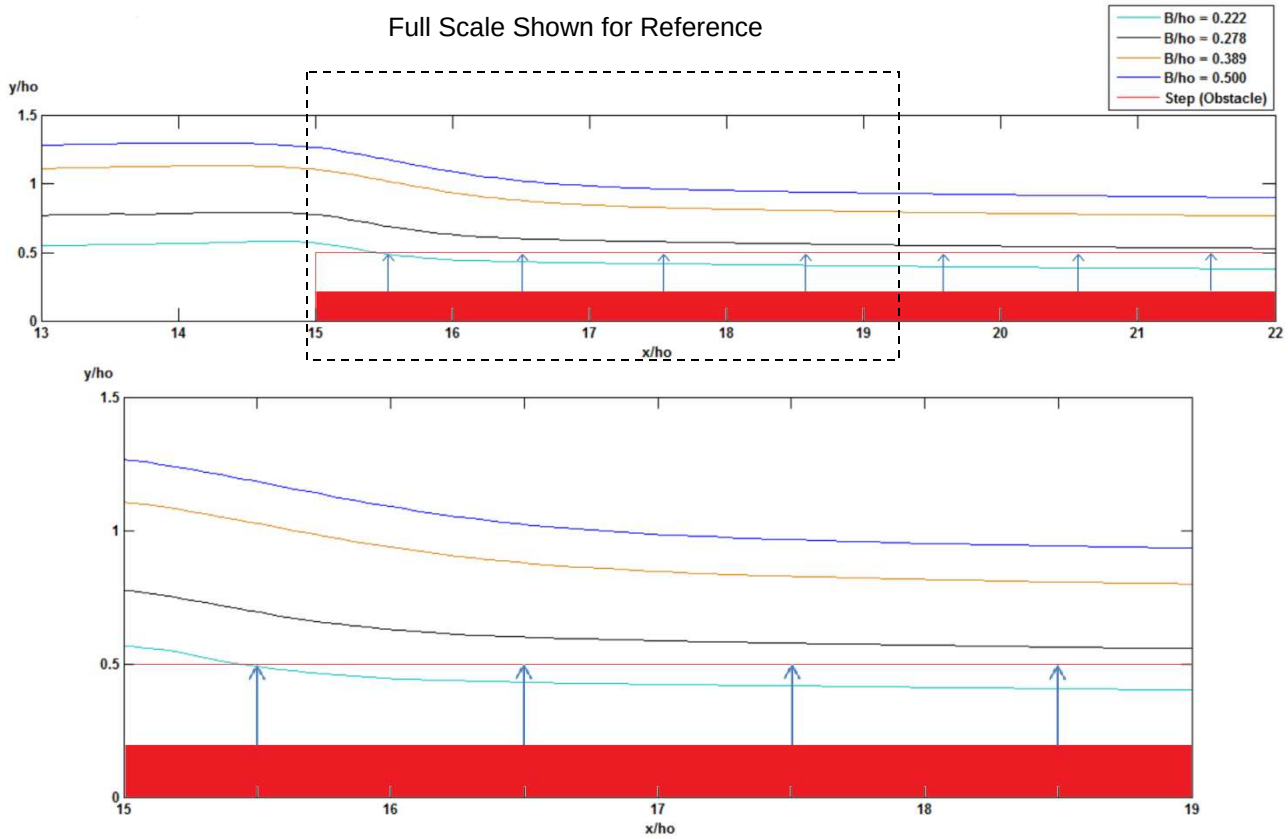

Figure 4.23 Testing results for a Sg = 2.443% and Fr_O = .45 with increasing step height.

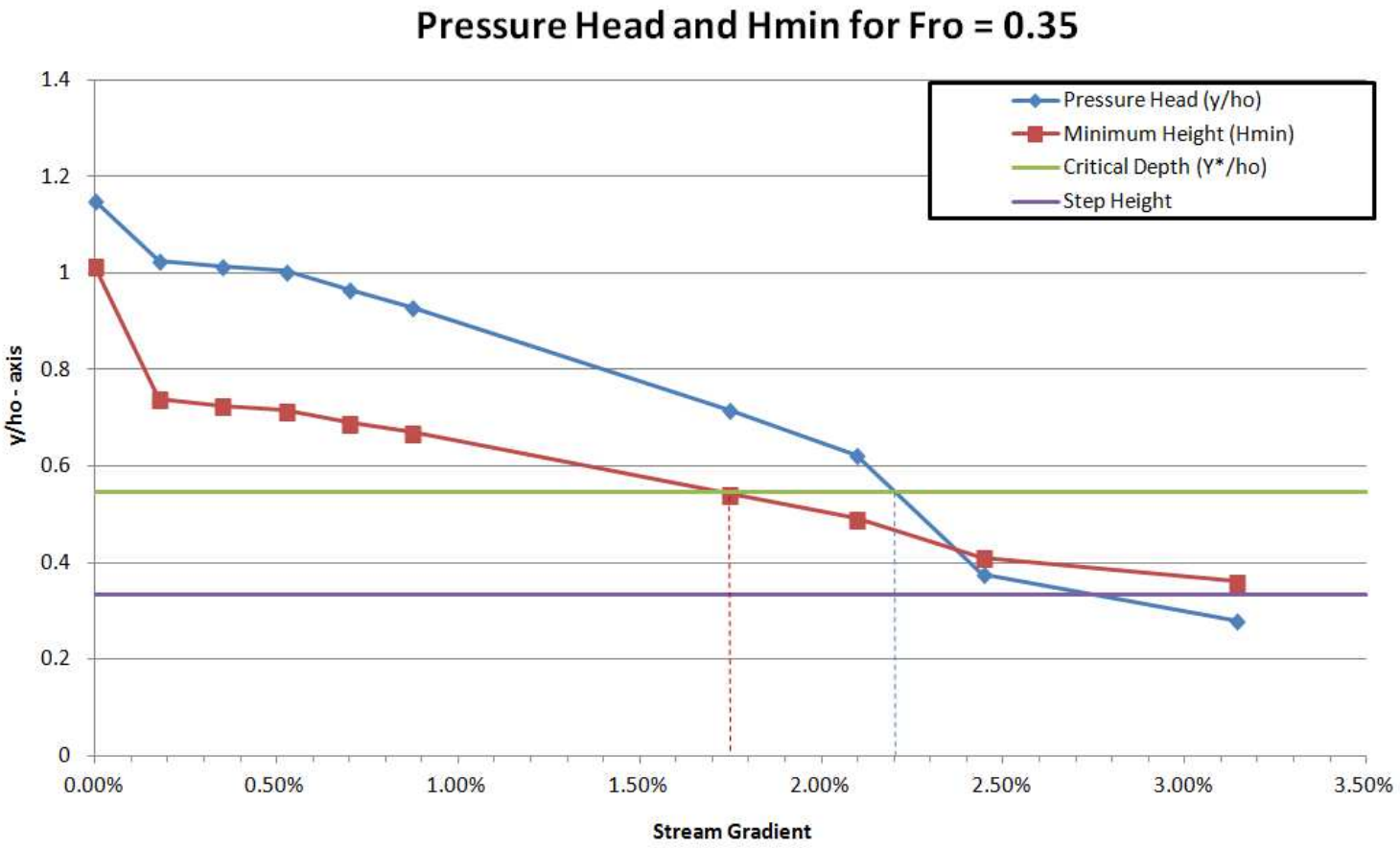

Figure 4.24 A critical depth analysis for Fro = 0.35.

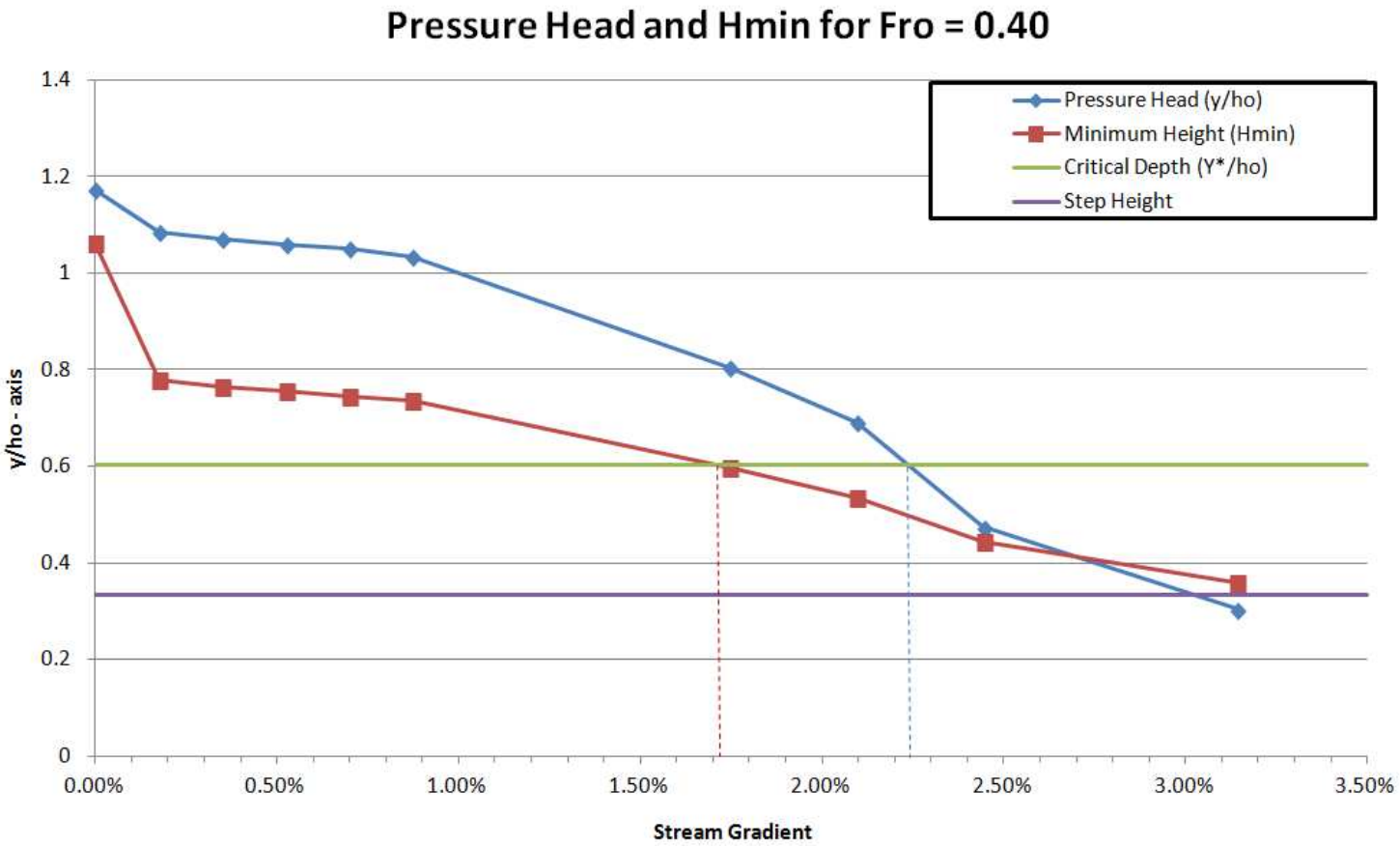

Figure 4.25 A critical depth analysis for Fro = 0.40.

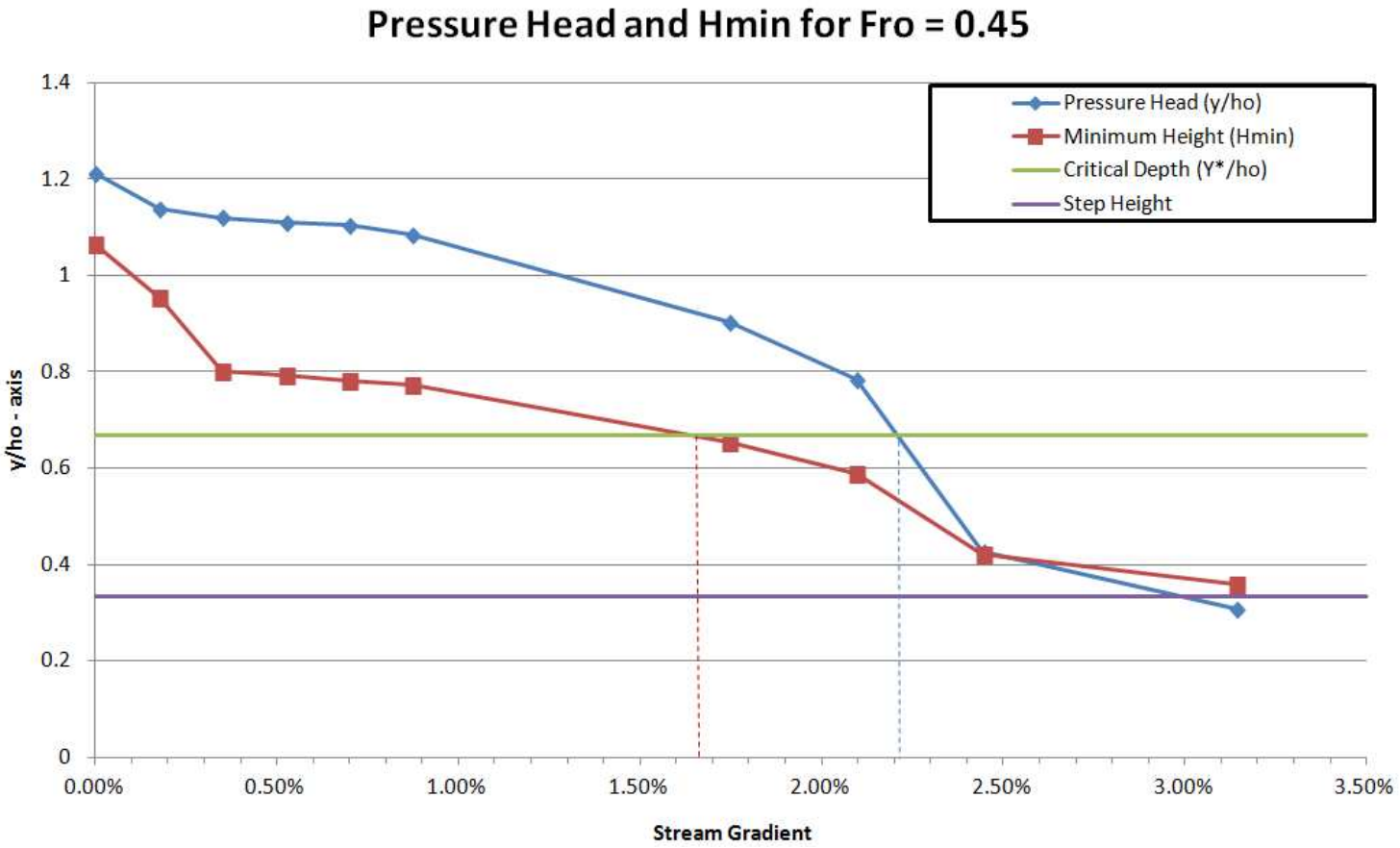

Figure 4.26 A critical depth analysis for Fro = 0.45.

Chapter 5

Conclusions and Future Research

5.1 Conclusion

A series of numerical simulations have been conducted in order to investigate the behavior of the free surface in response to an increasing stream gradient. As the shallow water equations have been found to be inaccurate for an obstacle such as a step a finite difference method employing a robust coupled level set – volume of fluid (CLSVOF) algorithm has been used to simulate the flow. The preliminary testing confirms the accuracy of the results when compared with experimental data. In the first series of testing the free surface behavior is observed for an increasing stream gradient. It is clearly seen that even a very low stream gradient can have an impact on the free surface behavior above the step. As the stream gradient becomes moderate the effect on the free surface becomes even more significant. This clearly shows that the stream gradient cannot be neglected in the case of open channel flow over a step. The pressure head and minimum height of the free surface are directly related to each other. It has been shown that there is a decrease in the height of Hmin as the stream gradient is increased which changes slowly at first, but will soon begin to change quickly as the stream gradient is increased. A critical depth analysis also reveals that the minimum depth of the free surface would reach the critical depth much sooner when the incident flow velocity is increased.

The next parametric study was for a constant stream gradient, and observed the change in free surface profiles as the incident flow velocity was increased. This study demonstrated that the free surface will experience a drop in pressure head that will cause the effect of the incident flow velocity to become more significant. As the stream gradient is increased the incident flow velocity will cause a greater rise in the height of the free

surface above the step. A set of simulations have been done to study the effect of the step height on the free surface of a flow over a downhill slope. These tests illustrate that the drop in pressure head will be counteracted by the increasing step height which will cause the height of the free surface to increase.

5.2 Future Work

Now that the results have been shown and discussed the future of this research is to improve the accuracy of the estimation of the free surface. It can be seen in Figure 4.9 that the results are in good agreement with the experimental results, but there is still some room for improvement. Flow separation is one factor that causes the wavy pattern of the free surface profile in the experiments of [1] to be more pronounced than the profile of the numerical simulation shown in Figure 4.9. A photo the of the flow from the experiments in [1] shows that in a real flow there would be a stagnation zone that manifests ahead of the step in addition to flow separation above the step such as shown in Figure 4.27. The vertical dimension of the flow separation can be a significant part of the flow depth which will produce a more wave like pattern in the free surface. The boundary conditions prescribed for BC1 and BC2 that are shown in Figure 3.4 are the second factor which will affect the accuracy of the simulation because as Fr_0 increases the pressure head near the inlet will increase in response.

The boundary conditions of the step at OB1 and OB2 shown in Figure 4.9 are prescribed to be rigid free-slip, and will neglect wall friction which is a significant factor in the formation of the separation zone. In future studies it is recommended that the boundary conditions that are prescribed for OB1 and OB2 be for a rigid no-slip condition in order to improve the accuracy of the results. In order to handle the increase in pressure head at the inlet there are two possible solutions that could be implemented. The first would be to use a deformable grid in the vertical direction such as used in [1],

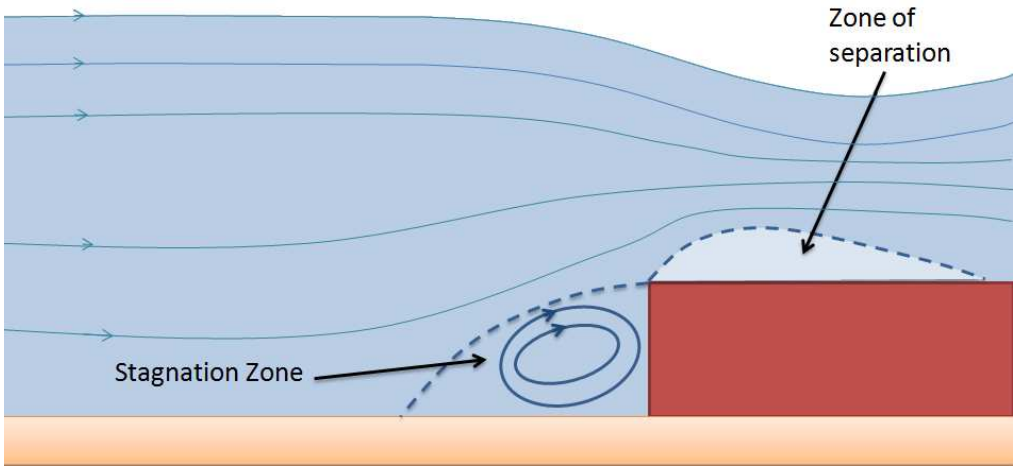

Figure 4.27 A depiction of a realistic flow with a separation zone and stagnation zone.

but this is not currently possible with the computational software used in this study. The second solution would require an algorithm be implemented at the boundary conditions of BC1 and BC2. In the current method the number of cells that are open to flow along the boundary of BC1 are fixed, and in Figure 4.28a we see that cell A remains closed to flow even though that fluid has begun to fill the cell. In the improved algorithm cell A would remain closed to flow if the VOF function remains less than 1 such as shown in Figure 4.28b. When the VOF value of cell A becomes equal to 1 the cell would be open to flow as shown in Figure 4.28c. This simple algorithm for the cells contained in BC1 and BC2 is summarized below:

$$C(\vec{x},t)=\begin{cases}1, & \text{Cell is open to flow from the inlet}\\ 0<C<1, & \text{Cell is closed to flow from the inlet}\end{cases} \tag{5.1}$$

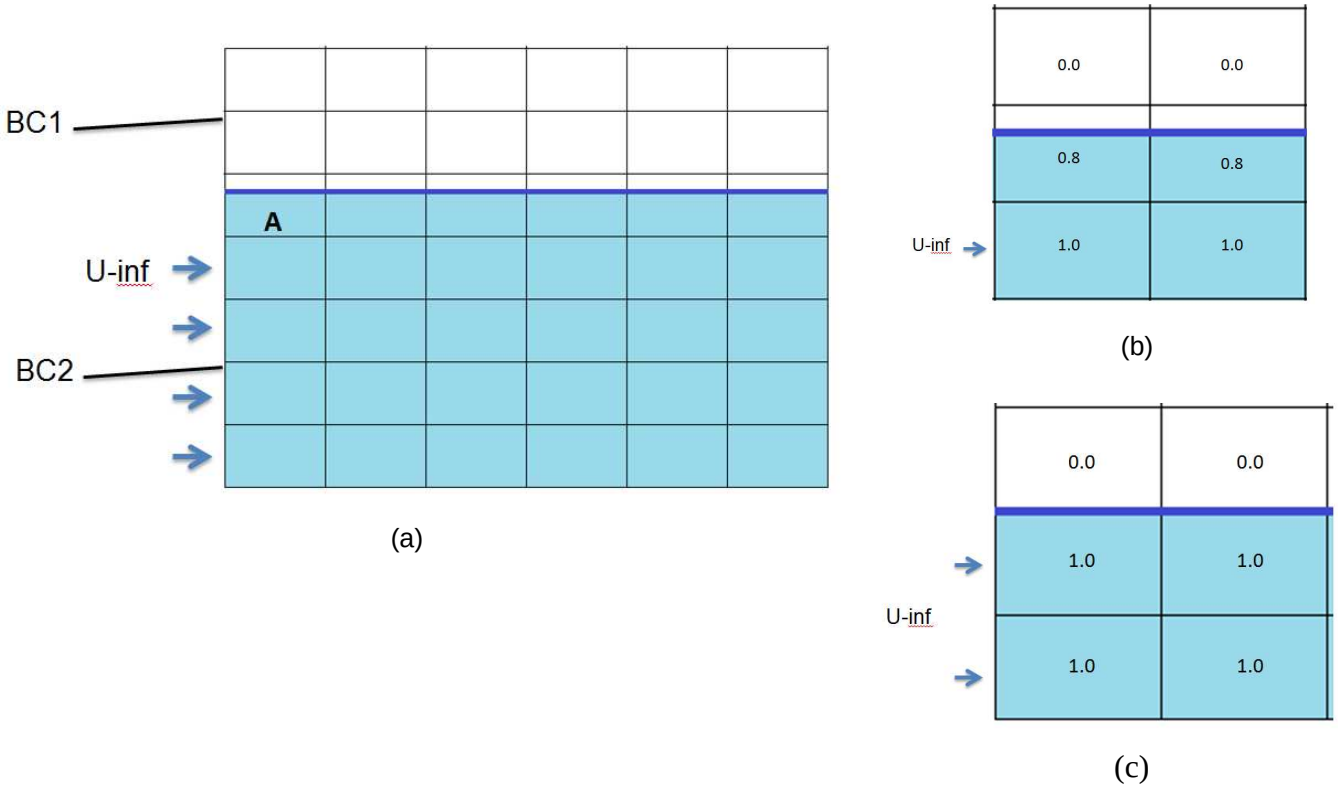

Figure 4.28 The cell layout (a) of the boundary conditions at the inlet and cell **A** located at the interface. Cell **A** in the new algorithm is closed to flow from the inlet when the VOF function is less than 1 (b) and open to flow from the inlet when the VOF function is equal to 1 (c).

Appendix A

Code Execution

A.1 Execution of Code

The code that was used in this study was written with a Fortran programming language in UNIX environment. A high performance computing system (*www.uta.edu/oit/eos/hpc/*) was used to run the program code for a computational fluid software called RIPPLE. The numerical simulations require four file placed in a destination directory:

- *file_name.dat*
- *input*
- *bjob*
- *ripple*

After these files are placed in the directory a job number created and the job is placed in a queue to await execution. The *file_name.dat* file contains a list of the name and number of all the locations to write the output data. The *input* file contains all of the information regarding the geometry, fluid properties, boundary conditions, numerical parameters, etc. A sample of an *input* file that was used is provided in Appendix B. The *bjob* file contains the load sharing facility instructions (LSF) that will specify which queue the job will placed in, what to name the job, and where to find the ripple executable code. The final file is the *ripple* executable file which contains the CLSVOF algorithm that will be used to execute the numerical simulation.

Appendix B

Sample Input and Output

B.1 Sample Input File

A sample of an *input* file used in a numerical simulation for this study is shown below:

```
11 Peter-Final 120212-Trial#47C10-#32 CLS [mm,ms,mg,K]
 $numparam
  alpha=2.0,
  autot=1.0,
  conserve=.false.,
  delt=0.150352953996178,
  dtmax=5.2624,
  twfin=800000,
  con = 0.3,
  fcvlim=0.5,
  idiv=1,
  dmpdt=300000000.0,
  prtdt=100000000.0,
  pltdt= 100000.0,
  ppltdt= 1.0,
  pperiod= 1.0,
  pstart= 200000000000.0,
  sym=.true.,
  kt =6,
  kb =3
  kl =2,
  kr =2,
  gfnctn=.true.,
 $end
 $fldparam
  gx= -9.81e-3,
  icyl=0,
  canglel=90, cangler=90, canglet=90, cangleb=90,
  isurf10=1,
  psat=0.0,
  xnu=1.005e-3,
  rhof=1.0,
  sigma=7.27e-2,
  vi=-0.477887843099613,
  vinf(2)=-0.477887843099613,
 $end
 $mesh
  nkx=1,
  xl = 0.0, 210.166658,
  xc= 105.083329,
  nxl = 13,
  nxr = 13,
  dxmn= 8.083333,
  nky=1,
  yl= 0.0, 5092.49979,
  yc= 2546.249895,
  nyl= 315,
  nyr= 315,
```

```
  dymn= 8.083333,
$end
$obstcl
  nobs=2,
    oa1(1)= 1.0, oc1(1)=  -48.499998, ioh(1)=1,
    ob1(2)=-1.0, oc1(2)=      2909.99988, ioh(2)=0,
$end
$freesurf
  nfrsrf=2,iequib=0,
  fc1(1)=-1.0, ifh(1)=0,
  fa1(2)= -1.0,fc1(2)= 145.499994,ifh(2)=1,
$end
$graphics
  plots=.true., dump=.false.,
  iout = 0, 1, 0, 0, 0, 0, 0, 0, 0, 0, 0, 0, 0,
        0, 0, 0, 0, 0, 0, 0,18, 21, 0, 0, 0, 0,
        0, 0, 0, 0, 0, 0, 0, 1, 0, 1, 1, 0, 1,
$end
$coupled
  lsvof=.true.,
  ls = .false.,
$end
```

B.2 Sample Output

The data file that is created during the simulation contains the time parameter, the first and last real cells in the (x) and (y) direction, the location of the left side of each computational cell in the (x) direction, the location of the lower side of each computational cell in the (y) direction, the velocities components, VOF value, LS value, enthalpy, and pressure. A sample of the data contained in the output is shown below along with an explanation of the organization of the data array:

```
0.00000E+000  <-------- time
 2, 26        <-------- 1st real cell, and the last cell in the (x) direction
 2,630        <-------- 1st real cell, and the last cell in the (y) direction
0.00000E+000 <-------- location of the left side of each computational cell in the (x)
8.08333E+000          direction
1.61667E+001
2.42500E+001
3.23333E+001
4.04167E+001
……
0.00000E+000 <-------- location of the left side of each computational cell in the (y)
8.08333E+000          direction
1.61667E+001
2.42500E+001
3.23333E+001
```

4.04167E+001
……
0.00000E+000, *0.00000E+000,* *0.00000E+000,* *-8.48549E+001,*
(Column 1) (Column 2) (Column 3) (Column 4)

0.00000E+000, *0.00000E+000*
(Column 5) (Column 6)

The six column array contains the solutions of the governing equations:

- Column 1: Velocity component in the (x) direction
- Column 2: Velocity component in the (z) direction
- Column 3: VOF function Value
- Column 4: LS function Value
- Column 5: Enthalpy
- Column 6: Pressure

References

[1] Bukreev, V. I., and Gusev, A. V.,"WAVES BEHIND A STEP IN AN OPEN CHANNEL", *Journal of Applied Mechanics and technical physics*, Vol. 44, No. 1, pp. 52-58, 2003.

[2] Khazhoyan, M.G., and Khakimzyanov, G.S., "NUMERICAL MODEL OF AN IDEAL INCOMPRESSIBLE FLUID FLOW OVER A STEP", *Journal of Applied Mechanics and Technical Physics, Vol. 47, No. 6, pp. 785–789, 2006*

[3] Peskin, C.S., "Numerical analysis of blood flow in the heart", *J. Comput. Phys.*,Vol.25 pp. 220-252, 1977.

[4] Sutherland, B.R., and Aguilar, D.A., "Stratified Flow over Topography: Wave Generation and Boundary Layer Separation", Department of Mathematical and Statistical Sciences, University of Alberta Edmonton, Canada.

[5] Martinuzzi, R., and Tropea, C., "The Flow Around Surface-Mounted, Prismatic Obstacles Placed in a Fully Developed Channel Flow", *Journal of Fluids Engineering*, Vol. 115, pp. 85-92,1993.

[6] Stüer, Heinrich, "Investigation of separation on a forward facing step", Ph.D. Dissertation, Swiss Federal Institute of Technology Zürich, University of Essen. Geimany, 1999.

[7] Saleel, C.A., Shija, A., and Jayaraj, S., "NUMERICAL SIMULATION OF FLUID FLOW OVER A FOWARD-BACKWARD FACING STEP USING IMMERSED BOUNDARY METHOD", *International Journal of Engineering Science and Technology*, Vol. 3 No. 10, October 2011.

[8] Su ,C. H., and Gardner, C. S. , ''Korteweg-de Vries equation and generalizations. III. Derivation of the Korteweg-de Vries Equation and Burgers Equation,'' J. Math. Phys. 10, pp536, 1969.

[9] Nadiga, B.T., and Margolin, L.G., "Different approximations of shallow fluid flow over an obstacle", *Phys. Fluids 8 (8)*, pp 2066-2077, August 1996.

[10] Harlow, F. H.,Welch, J. E., "Numerical calculation of time-dependent viscous incompressible flow of fluid with a free surface", *Physics of Fluids 8,* pp 2182–2189, 1965.

[11] Noh, W.F., Woodward, P., "SLIC (Simple Line Interface Calculation). In proceedings of 5th International Conference of Fluid Dynamics, edited by A. I. van de Vooren & P.J. Zandbergen", *Lecture Notes in Physics Vol. 59,* pp 330–340, 1976.

[12] Hirt, C. W. and Nichols, B. D., “Volume of Fluid (VOF) Method for the Dynamics of Free Boundaries,” Journal of Computational Physics, Vol. 39, pp. 201-225, 1981.

[13] Youngs, D. L., "Time-dependent multi-material flow with large fluid distortion", *Numerical Methods for Fluid Dynamics*, Academic Press, New York, pp 273-285, 1982.

[14] Sethian, J.A., “Level Set Methods: Evolving interfaces in geometry, fluid mechanics, computer vision, and material science”, Cambridge University Press, 1996.

[15] Osher, S. J., Fedkiw, R.P., “Level Set Methods and Dynamic Implicit Surfaces”, Springer-Verlag, New York, Inc., 2003

[16] Brackbill, J.U., Kothe, D.B., Zemach, C., "A continuum Method for Modeling Surface Tension",Journal of Computational Physics, Vol. 100, pp 335-354,1992.

[17] Kothe, D. B., Mjolsness, R. C., and Torrey, M. D., “RIPPLE: A computer program for incompressible flows with free surfaces”, Technical Report, LA-12007-MS, Los Alamos National Laboratory, 1991.

[18] Kershaw, D.S., “The Incomplete Cholesky-Conjugate Gradient Method for the Iterative Solution of Systems of Linear Equations”, *Journal of Computational Physics,* Vol. 26, pp 43-65, 1978.

[19] Sussman, M. and Fatemi, E., “An efficient, interface-preserving level set re-distancing algorithm and its application to interfacial incompressible fluid flow”, *SIAM J. Sci. Comput.,* vol.20, No. 4, pp 1165-1191,1999.

[20] Son, G. and Hur, N., “A coupled level set and volume-of-fluid method for the buoyancy-driven motion of fluid particles, Numerical Heat Transfer, part B, Vol. 42, pp 523-542, 2002.

[21] Wang, Z., "NUMERICAL STUDY ON CAPILLARITY- DOMINANT FREE SURFACE AND INTERFACIAL FLOWS", Ph.D. Dissertation, Department of Mechanical Engineering, The University of Texas at Arlington, TX, 1995.

[22] Lord, M.L., Germanoski, D., Allmendinger, N. E., "Fluvial geomorphology: Monitoring stream systems in response to a changing environment", Geological Monitoring: Boulder, Colorado, Geological Society of America, p. 69–103, 2009.

[23] "Appendix III-A Descriptions of Channel Habitat Types", Oregon Watershed Assessment Manual, Oregon Watershed Enhancement Board, Oregon, 1999.

Biographical Information

Peter Martinez was born and raised in Benbrook, Texas. He grew up in the DFW area and worked in cell phone repair and distribution until deciding to attend the University of Texas at Tyler where he received his B.S. in Mechanical Engineering in May of 2010. Originally seeking to pursue a career in the Power Industry, to work at a power plant like his father, his academic studies concentrated on the Thermal and Fluid Sciences. After graduation he enrolled in graduate school to begin the pursuit of his M.S. in Mechanical Engineering at the University of Texas at Arlington. He is now planning to enroll in the PhD program at UT-Arlington to continue his research.